

Polymer electrolytes in strong external electric fields: Modification of structure and dynamics

Alina Wettstein,^{*,†} Diddo Diddens,[‡] and Andreas Heuer^{*,‡,†}

[†]*Institut für physikalische Chemie, Westfälische Wilhelms-Universität Münster, Corrensstraße 28/30,
D-48149 Münster, Germany*

[‡]*Institut für Energie- und Klimaforschung, Ionics in Energy Storage, Helmholtz Institut Münster,
Forschungszentrum Jülich, Corrensstraße 46, 48149 Münster, Germany*

E-mail: alina.wettstein@gmail.com; andheuer@wwu.de

Abstract

We present the results from an extensive atomistic molecular dynamics simulation study of poly(ethylene oxide) (PEO) doped with various amounts of lithium-bis(trifluoromethane)sulfonimide (LiTFSI) salt under the influence of external electric field strengths up to 1 V/nm. The motivation stems from recent experimental reports on the nonlinear response of mobilities to the application of an electric field in such electrolyte systems and arising speculations on field-induced alignment of the polymer chains, creating channel-like structures that facilitate ion passage. Hence, we systematically examine the electric field impact on the lithium coordination environment, polymer structure as well as ionic transport properties and further present a procedure to quantify the susceptibility of both structural and dynamical observables to the external field. Our investigation reveals indeed a coiled-to-stretched transformation of the PEO strands along with a concurrent nonlinear behavior of the dynamic properties. However, from studying the temporal response of the unperturbed electrolyte system to field application we are able to exclude a structurally conditioned enhancement of

ion transport and surprisingly observe a slowing down. A microscopic understanding is supplied.

To meet the ever increasing need for electrochemical energy storage systems in the context of progressive orientation on a sustainable and mobile energy supply, scientific focus remains on the improvement of lithium-ion battery technology.¹ As an alternative to the state-of-the-art liquid electrolytes, setting the standard for ionic conductivities but bearing safety risks associated amongst others with electrolyte decomposition,²⁻⁴ solid polymer electrolytes provide inherently robust mechanical properties, which are required for the diverse ambient conditions that batteries are deployed in. The most investigated solid polymer electrolyte material is an amorphous poly(ethylene) oxide (PEO) matrix dissolving a lithium salt, for example lithium-bis(trifluoromethane)sulfonimide (LiTFSI).⁵⁻⁹ However, the contemporary achievable ionic conductivity at ambient temperatures is still too low to compete in technological application, which hence further fuels the necessity to fully understand the transport behavior in these systems.^{8,10,11}

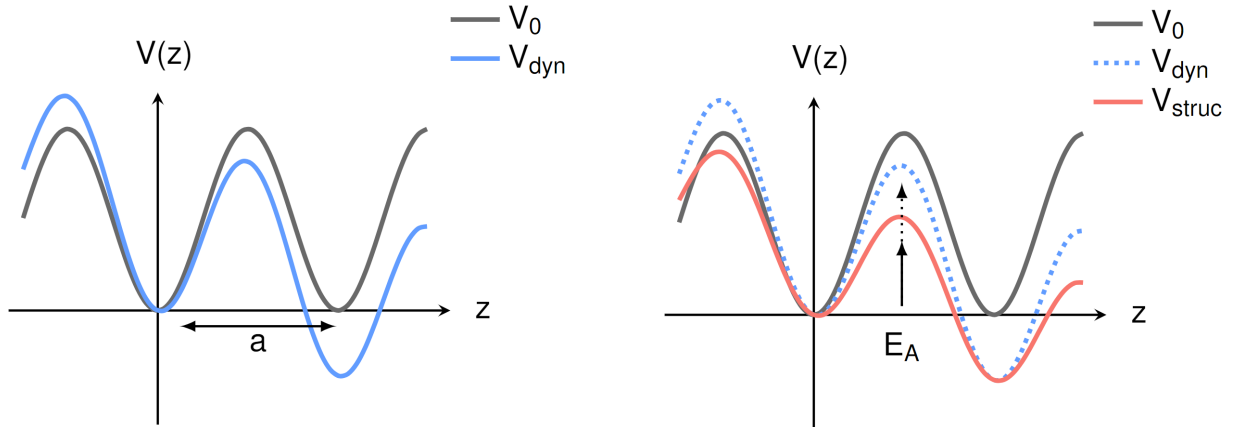


Figure 1: Sketch of one-dimensional potential energy profile $V(z)$ in direction of the electric field. Left: Effective lowering of activation barriers E_A due to tilting of energy surface in field direction. Right: Additional decrease of barrier heights due to structural modifications.

Studying the impact of electric fields on polymer electrolyte systems emerges as highly relevant in regard to the electrode/electrolyte interfaces where ionic concentration gradients

evoke local potential drops that correspond to local field strengths in the order of volts per nanometer.^{12–15} Strong electric fields may further be induced by dendritic lithium structures that form upon cycling the battery and pierce through the polymer host matrix.^{16–18}

Both experimental^{19–21} and theoretical²² research on ion transport in polymeric systems in the presence of an external electric field have indicated a nonlinear enhancement of ion dynamics. Based on the observation of field-dependent mobilities in electrophoretic NMR measurements carried out at electric field strengths $\mathcal{O}(10 \text{ V/cm})$ Rosenwinkel et al. put forward the hypothesis of evolving polymer channel structures that guide ion transport efficiently.¹⁹ Even though this line of reasoning comes along as very intuitive, a causal understanding of such nonlinear effects can turn out much more complex. For instance, experimental and theoretical work on inorganic lithium silicate glasses detected a nonlinear response of lithium ion dynamics to an external field, yet the systems experienced no structural modifications.^{23–25} From the perspective of the potential energy surface two entirely independent effects may give rise to a field-induced enhancement of the dynamics. In Figure 1 we show a sketch of a potential energy profile in one dimension which is pictured for reasons of simplicity via a sinusoidal shape. In absence of an external field the ion vibrates in a potential well, that is a local minimum of the energy landscape. To migrate over a further distance, i.e. the width a of the potential well, the ion requires an activation energy E_A to overcome the potential barrier. While thermal fluctuations of the environment may enable such a crossing occasionally, the application of an external field effects an additional energy gain in field direction (see Figure 1 left). As a consequence, the energy profile is tilted such that the activation barriers for migration in field direction are lowered (respectively raised for backward jumps) which hence causes an increasingly directed ion motion. Mathematically, one can capture the biasing effect of the field on forward and backward jumping rates $\Gamma_{f/b}$ through an additional energy contribution in the Boltzmann factor:^{26,27}

$$\Gamma_{f/b} = \Gamma_0 \cdot \exp\left(\pm \frac{qEa}{2k_B T}\right), \quad (1)$$

where Γ_0 denotes the undirected jumping rate without field and q the charge of the particle which is forced by the external field E . A Taylor expansion of the thus stated hyperbolic sine dependence of the ion drift velocity ν on the external field naturally yields a nonlinear transport behavior for sufficiently high fields:^{22,26,27}

$$\langle \nu \rangle = \frac{d}{dt} \langle z \rangle = a (\Gamma_f - \Gamma_b) = a \Gamma_0 \sinh \left(\frac{qEa}{2k_B T} \right) = t_1 \cdot E + t_3 \cdot E^3 + \dots \quad (2)$$

If the field furthermore induces structural changes that cause an additional decrease of the potential barriers (see Figure 1 right), the nonlinear response may either be complementary enhanced or even dominated by such structural modifications.

In this work, we address three questions by means of atomistic molecular dynamics (MD) simulations covering a broad range of electric field strengths: Does the field alter structural and/or dynamical properties of the salt-in-polymer electrolyte? If so, at which field strengths and how pronounced do these effects occur? Is the nonlinear increase of transport properties conditioned by such conformation changes in this soft matter system?

The paper is organized as follows: First, we present our results on the ion dynamics as a function of field strength. Then, we discuss the lithium coordination environment and the polymer chain structure under field application. Next, we bring forward an explanatory approach to rationalize the structuring of the polymer host matrix and further develop a concept to classify the field susceptibility of both structural and dynamic observables. Lastly, we discuss the correlation between structure and dynamics on the basis of field-switch simulations and close with an overall conclusion.

Simulated systems

The MD simulations were performed with the GROMACS²⁸⁻³¹ software package relying on the classic all-atom, non-polarizable OPLS-AA and OPLS-AA-based CL&P force field³²⁻³⁶ at a temperature of 423 K. The details of the structure generation and simulation protocol are given in the *Supporting Information* section. Inspired by the experimental study

of Rosenwinkel et al. the integral part of our study covers three salt-in-PEO electrolyte systems with salt-to-monomer ratios $r = [\text{Li}]/[\text{EO}] = 0.06, 0.10$ and 0.15 . Each system contains 20 coiled PEO chains composed of $N = 27$ monomer units and the corresponding amount of LiTFSI ion pairs (36, 54 and 81 Li/TFSI molecules). Beyond that a variety of slightly modified setups was simulated to answer questions arising in the course of this investigation. These include a plain polymer melt ($r = 0.0$) as well as an artificial scenario ($r = 0.06$) where only lithium and TFSI experience an external electric force to capture the purely ionic response to the field. To determine if the occurrence of field effects is limited by the molecular weight of the polymer chains, we investigated an $r = 0.06$ electrolyte mixture containing 10 coiled PEO chains double in length, i.e. $N = 54$. Furthermore, we performed a series of 100 short (5 ns) simulations where an electric field of 1 V/nm is applied on $E_z = 0.0$ V/nm structures of the $r = 0.06$ mixture to trace how structural and dynamical observables equilibrate to their steady state value. All simulation trajectories were run for at least 300 ns and cover up to $2 \mu\text{s}$ to ensure that the diffusive regime has been reached.

Dynamical properties. We investigate the impact of the electric field on ion dynamics on the basis of the electrophoretic mobilities μ , as measured in the electrophoretic NMR experiments,¹⁹ and diffusion coefficients in field direction D_{\parallel} , i.e. the diffusion within the moving coordinate frame of reference that is constituted by the drift motion. We extract

$$\mu = \frac{\langle \nu \rangle}{E} = \lim_{t \rightarrow \infty} \frac{z(t) - z(0)}{E \cdot t} \quad (3)$$

from the ion's stationary drift velocity ν . In order to assess the diffusion coefficient in field direction, we analyze the parallel component of the mean-square displacement (MSD) in the moving coordinate frame:^{37,38}

$$D_{\parallel} = \lim_{t \rightarrow \infty} \frac{\text{MSD}_{\text{parallel}} - \langle \nu \rangle^2 \cdot t^2}{2 \cdot t}. \quad (4)$$

For small electric fields, i.e. small perturbations from equilibrium, it is expected that neither

μ (see equation (2)) nor D_{\parallel} depend on E_z . Thus any deviation from the linear response can be directly interpreted as a nonlinear effect. Since the Einstein relation connecting diffusion constant and mobility has been found to no longer hold beyond the linear response regime even in systems without ion correlations,³⁸ the influence of the electric field on D_{\parallel} is a priori unknown. Therefore, investigation of D_{\parallel} provides novel information on the complexity of the nonlinear dynamic effects.

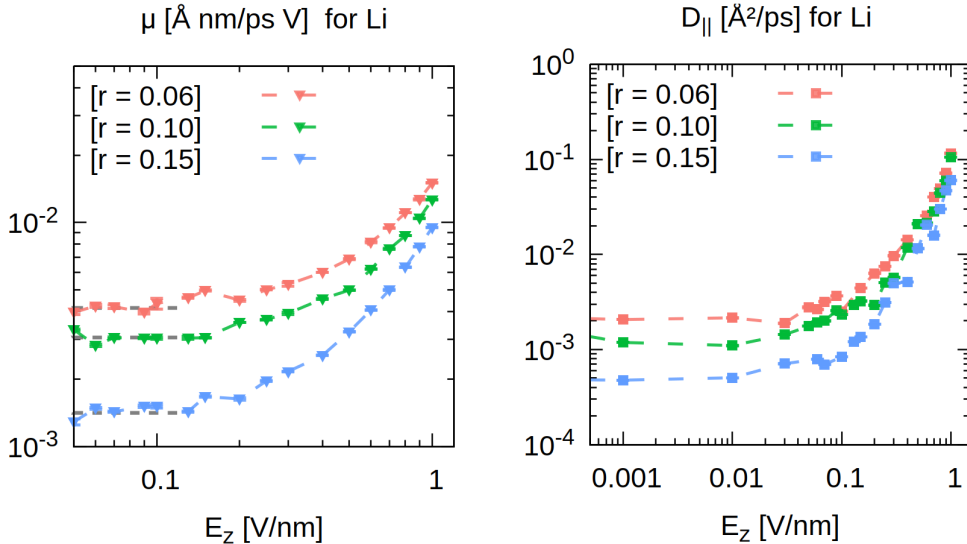


Figure 2: Lithium mobilities μ and parallel diffusion constants D_{\parallel} as a function of electric field strength for three different salt concentrations. The dashed grey horizontal lines mark the linear response mobilities at the respective concentration, which were employed to evaluate D_{\parallel} for $E_z < 0.03$ V/nm.

The resulting mobilities and diffusion coefficients for lithium are shown in Figure 2 (see Figure S3 for TFSI dynamics). For application of an electric field we observe a substantial enhancement of μ and D_{\parallel} for both ion species, whereas the impact is more pronounced for D_{\parallel} , which is increased by nearly two orders in magnitude. Interestingly, ranking the intensity of the enhancements of μ and D_{\parallel} in this soft matter system matches the observations that have been made previously on lithium silicate glasses.²³⁻²⁵ Demonstrating a strong similarity to such inorganic glasses, the threshold electric field strengths to observe nonlinear effects in our simulation, i.e. $E_z \gtrsim 0.2$ V/nm for μ_{Li} and $E_z \gtrsim 0.05$ V/nm for $D_{\parallel\text{Li}}$, lie considerably

above the electric field strengths $\mathcal{O}(10 \text{ V/cm})$ employed in the eNMR measurements.

We note that in absence of an external field the diffusion coefficients for both lithium and TFSI for the $r=0.06$ mixture are in accordance with simulations of an amorphous LiTFSI-PEO melt ($r=0.06$, $T=416 \text{ K}$) employing a many-body polarizable force field.³⁹ Furthermore, the transport properties decrease in magnitude for increasing salt concentration as expected from the increasing viscosity.^{40,41} Due to the strong interactions between lithium and the polymer ether oxygens lithium is less mobile and as a result less diffusive than TFSI despite its smaller size.^{19,40,41}

To ensure within the realms of simulation work that our observations of enhanced transport properties induced by the electric field are not limited by the molecular weight of the simulated chains, we performed additional simulations for the $r=0.06$ electrolyte employing chains double in length. We show in the Supplementary Information section that nonlinear dynamics are observed for this system as well. A closer discussion of the chain length dependence is, however, beyond the scope of this work.

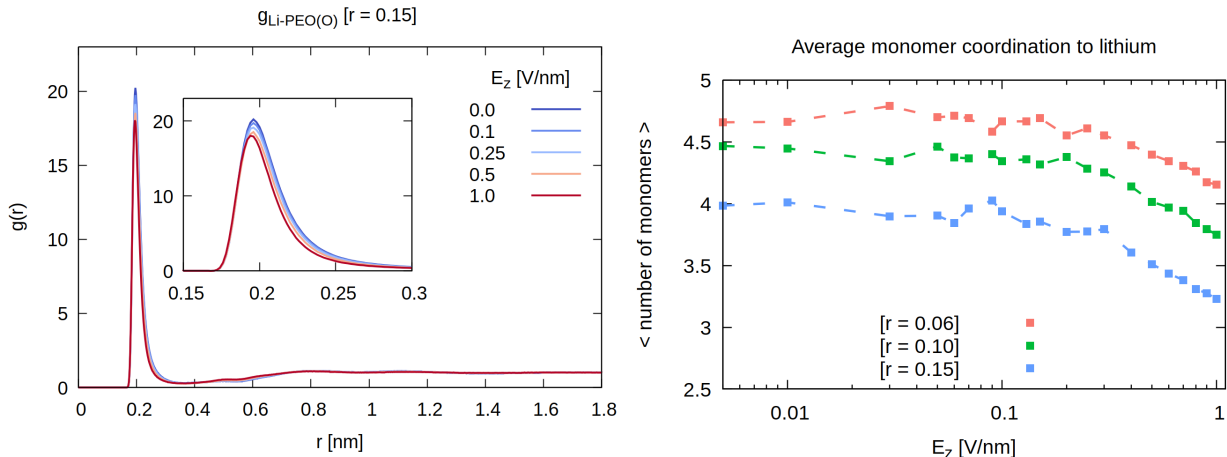


Figure 3: Left: Exemplary lithium-ether oxygen radial distribution function for a variety of electric field strengths E_z for the Li[TFSI]-PEO mixture with a monomer-lithium ratio $r=0.15$. Right: Average lithium-monomer coordination number as a function of electric field strength.

Lithium coordination environment. To ascertain whether the electric field modifies the structural properties of the lithium salt-polymer system, we investigate the lithium

coordination environment. The radial distribution functions $g_{\text{Li-PEO(O)}}(r)$ of polymer oxygens around lithium as a reference are shown in Figure 3 exemplary for the $r = 0.15$ system for various E_z . In agreement with previous simulation studies the first sharp coordination peak for the lithium - ether oxygen bonds emerges at a distance of 2.0 Å while the second coordination sphere appears to be smeared at a distance of 4.5 Å.^{42,43} We observe that the peak heights decrease with increasing field strength which is indicative of a liberation of the lithium ions from the polymer backbone. Integration of $g_{\text{Li-PEO(O)}}(r)$ up to the first minimum yields the average number of monomers coordinating to lithium as shown Figure 3, which we find for all salt concentrations to decrease accordingly.

Table 1: Relative frequencies of chain coordination motifs in absence of electric field and a maximum electric field strength of $E_z = 1.0$ V/nm exemplary for $r = [\text{Li}]/[\text{EO}] = 0.06$ (see Table S1 for higher salt contents). The label 'free' means that lithium is not coordinated by the polymer. τ denotes the mean residence time of lithium on a polymer chain.

| E_z [V/nm] | free [%] | 1 chain [%] | 2 chains [%] | τ [ns] |
|--------------|----------|-------------|--------------|-------------|
| 0.0 | 0.5 | 96.9 | 2.6 | 263.4 |
| 1.0 | 3.0 | 81.3 | 15.7 | 2.8 |

Analysis of the lithium-polymer coordination data as a function of chain identity is provided in Table 1 and confirms primary coordination by a single polymer chain in the absence of an external field as ascertained in other simulation studies.^{39,44,45} We make the observation that under influence of an external field the coordinating monomers are increasingly provided by two different polymer chains (see simulation snapshot in Figure 4) and further, that a growing percentage of the lithium ions is structurally decoupled completely from the polymer at maximum field strength. We find further indication of such weakening attachment of lithium to the polymer in drastically declining mean residence times τ of lithium on the chain, which drop approximately two orders in magnitude (see Table 1). One might tentatively postulate that decreasing interaction of lithium and polymer, i.e. the decreasing coordination numbers as well as a breaking up of the typical crown-ether coordination cage that is provided by one polymer chain wrapping around the lithium ion, allows for more fre-

quent lithium transfers between the polymer chains and, eventually, accounts for the large increase of lithium mobility and diffusion.

We note that $g_{\text{Li-Li}}$ and $g_{\text{Li-TFSI(O)}}$ respond differently to field application as both probability distributions increase at smaller distances and thus yield lithium-TFSI and lithium-lithium coordination numbers increasing with field strength (see Figures S5-S8). We assess this as remarkable evidence of a structural reorganization induced by the electric field.

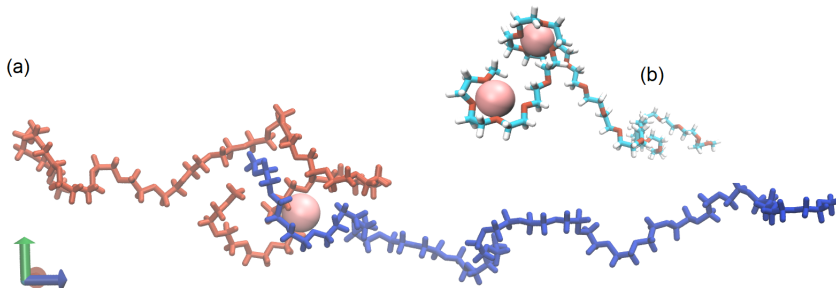


Figure 4: Top right: Snapshot of typical crown ether coordination environment of lithium via a single polymer chain. Bottom: Simulation snapshot of lithium coordinating to two polymer chains for $E_z = 0.9 \text{ V/nm}$. The blue axis points in z-direction.

Polymer structure. We analyze the conformational properties of the polymer chains in terms of the mean squared radius of gyration parallel ($R_{g,z}^2$) and orthogonal ($R_{g,x}^2$) to field direction. The results are depicted in Figure 5. Whereas the electric field hardly affects the chain elongation in x-direction, we observe that for exceeding a field strength $E_z = 0.1 \text{ V/nm}$ the chains start to expand in field direction in the lithium salt containing systems. We find that $R_{g,z}^2$ is increased more efficiently for decreasing salt content.

The ordering effect levels off at elevated field strengths and a maximum capacity of chain stretching can be observed. The final plateau is even more pronounced in the reference simulations containing polymer chains of double length as shown in Figure S21. The polymer chains exhibit a finite length, which naturally calls for a maximum elongation achievable within the respective conditions. The plain polymer does not display such a chain stretching behavior, but at most a slight trend of compaction in field direction.

We provide a microscopic understanding of this observation in the Supplementary In-

formation section S4, which can be briefly summarized as follows: As a consequence of counteracting orientation of the polymer monomers, which constitute a local dipole due to unequally distributed partial charges on oxygen and carbon atoms, the polymer chains are contracted in field direction. This effect counteracts the global chain alignment and may contribute to the decelerating trend of chain ordering at strong field strengths.

To clarify if the chain stretching originates from the polymer itself in the salt containing systems, we performed additional simulations for the $r = 0.06$ mixture, in which only lithium and TFSI experienced the electric field but not the partial charges of the polymer backbone. Figure S13 shows that the chains are equally stretched in this artificial scenario except for deviations at high electric field strengths close to 1 V/nm. We speculate that for these high fields the previously mentioned chain contraction originating from the polymer itself comes into effect and causes this discrepancy. Yet, we can conclude that the lithium salt causes the chain unfolding.

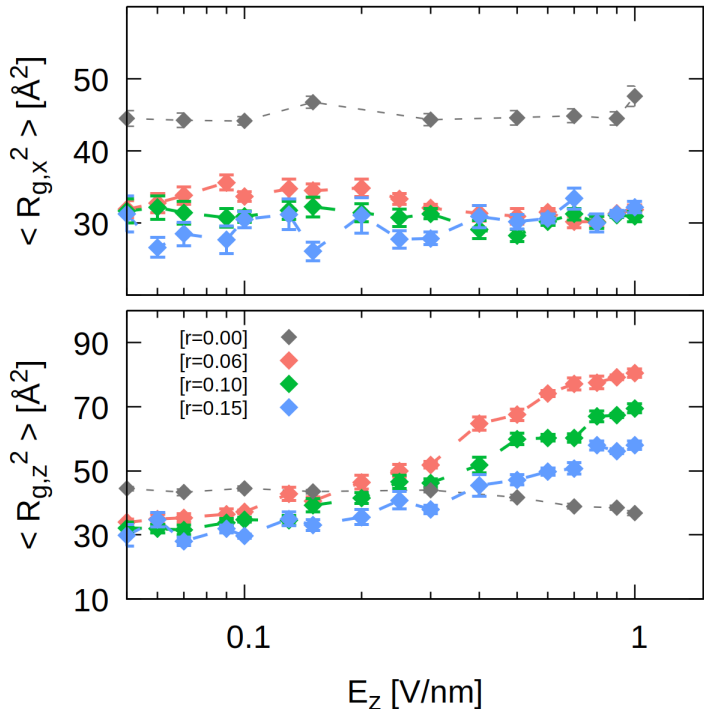


Figure 5: Polymer elongation as a function of electric field strength for various lithium salt concentrations. Mean squared gyration radii $R_{g,x}^2$ (top) and $R_{g,z}^2$ (bottom).

In the Supplementary Information section S6, we present a comprehensive discussion of the the coiled-to-stretched transformation of the polymer conformation, which we find to be induced by lithium, closely attached to the ether oxygens, pulling the polymer chain into the elongated shape. We note that the stretching is most efficient for an asymmetric distribution of the lithium ions along the polymer backbone, which hence serves as an explanation of a more effective chain alignment in field direction for decreasing salt content as observed in Figure 5. The probability for an asymmetric positioning of lithium on the polymer chains declines with increasing salt content (see Figure S20) and so does consequently the ability of the lithium ions to stretch the chains.

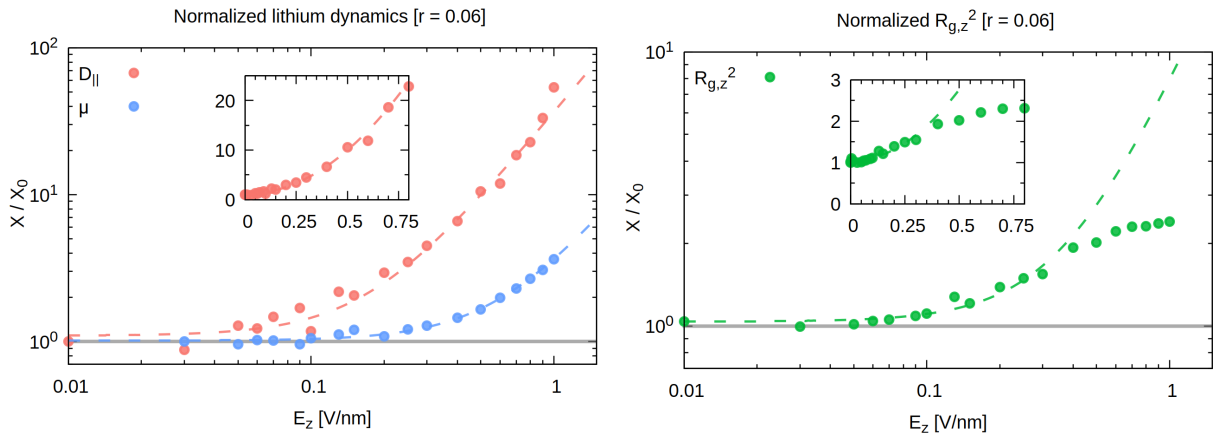


Figure 6: Deviation from the equilibrium value of lithium diffusion D_0 and polymer $R_{g,z,0}^2$ in absence of an electric field, respectively deviation from the force independent plateau mobility μ_0 in the linear response regime of the drift velocities. The dashed lines are the quadratic fits. Whereas $D_{\parallel}(E)$ and $\mu(E)$ are fitted over the entire field range, $R_{g,z}^2(E)$ is only fitted up to $E_z = 0.4$ V/nm once the effect of saturating chain order sets in.

Overall picture of field dependence. Since the response of either structural or dynamical properties $X(E)$ must be independent of the direction of the electric field (a reversal of the field causes solely a reversal of the drift direction), the field dependence can be captured by an even polynomial series:

$$X(E) = X_0 + \chi \cdot E^2 + \mathcal{O}(E^4), \quad (5)$$

i.e. in first approximation by a parabola, which recovers in the limit of small electric fields $E \rightarrow 0$ the quiescent value X_0 . We note in passing that for special systems also non-analytical terms, e.g. $a_1|E|$ may occur.²⁶ We show in Figure 6 exemplary for lithium that the dependencies of μ , D_{\parallel} and $R_{g,z}^2$ on E_z can be described by a quadratic fit. For better comparability the observables are normalized to their respective value in absence of an external field. We point out that the plateauing trend of $R_{g,z}^2$ is not reflected in a deceleration of the dynamic enhancements.

In order to enable a comparison between inherently different properties, such as the response of the gyration radius or parallel diffusion coefficients to the external field, we define a critical field strength E_c , which denotes a doubling of the observable in absence of a field, that is X_0 . This critical field strength thus may be extracted from the quadratic fit parameters (for example fits see dashed lines in Figure 6):

$$2 \cdot X_0 = X_0 + \chi \cdot E_c^2 \quad \Rightarrow \quad E_c = \sqrt{X_0/\chi}. \quad (6)$$

Figure 7 systematically summarizes the thus quantified degree of field-induced enhancement of the lithium dynamics and structural alterations, which we have touched before only in a qualitative manner. Note that none of the subsequent conclusions depend on the specific choice of the factor of 2 in equation (6).

First, we find that the critical fields E_c split into two domains, i.e. E_c values above and below 1 V/nm. It requires strong electric fields to alter the immediate lithium environment characterized in terms of oxygen coordination numbers. The coordination numbers display an increasing susceptibility to the field for increasing salt content. The nonlinear response of the lithium dynamics as well as the polymer chain alignment, on the other hand, occurs at considerably smaller field strengths. As stated previously D_{\parallel} features by far the strongest nonlinear effects. Whereas μ and D_{\parallel} follow the concentration dependence of the coordination numbers, the gyration radius $R_{g,z}^2$ ranging in a field regime in between displays the opposite

dependence on salt content. As we further recall that the plateauing trend of $R_{g,z}^2$ is not reflected in the field dependence of μ and D_{\parallel} , it seems implausible that $R_{g,z}^2$ conditions the transport enhancement. These observations suggest that there is, if at all, only a weak impact of structural modifications on the field-enhanced dynamics. However, no strict conclusions can be drawn on the causality of structure and dynamics since we may have missed to study the decisive structural quantity.

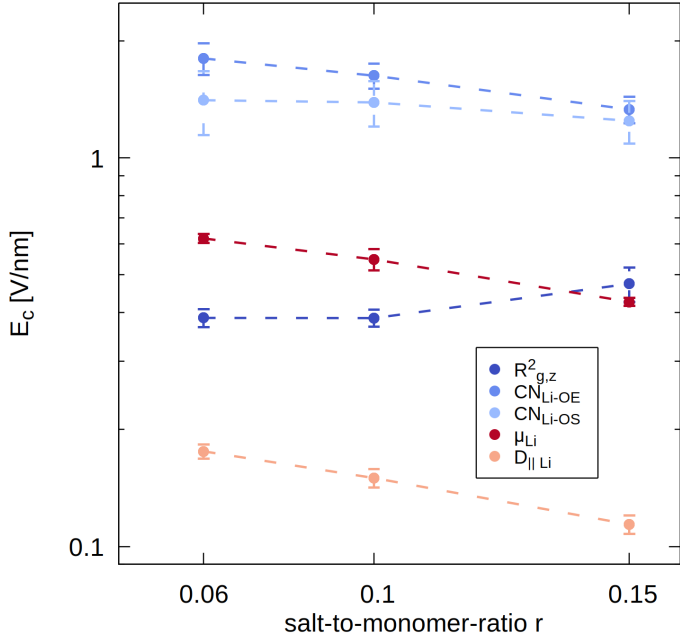


Figure 7: Critical field strengths E_c extracted from fitting the field dependence of dynamic transport (red) and structural (blue) properties via $X(E) = X_0 + \chi \cdot E^2$.

Field switching. Up to now our findings are based on the steady-state behavior of the electrolyte systems under influence of a static electric field, which has not yet yielded a firm conclusion about the possible causality between structural modifications and nonlinear dynamics. In order to discriminate the contributions to the nonlinear dynamics due to (1) tilting the energy landscape and, possibly, (2) structural alteration effecting a beneficial reshaping of the potential barriers, we investigate with temporal resolution the response of an equilibrium structure to perturbation via a strong electric field.

Our expectations on the temporal evolution of $\mu(t)$, assuming that structural modifica-

tions contribute to the dynamic enhancement, are qualitatively depicted in Figure 8. Tilting the energy landscape instantaneously lowers the activation barriers and thereby raises the linear response mobility μ_0 to μ_{dyn} . The structural impact comes into effect after a finite time, i.e. when the structural observable responds to the external field and relaxes to its steady-state value. Hence, we expect $\mu(t)$ to approach its steady-state value $\mu_{\text{dyn+struc}}$ concurrently from below.

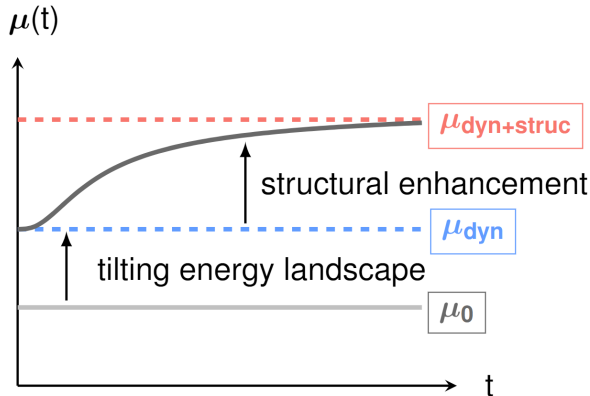


Figure 8: Sketch of anticipated time dependence of $\mu(t)$ for structurally conditioned enhancement of the dynamics.

Since our focus is now placed on the time dependence of lithium transport, μ can no longer be obtained from the long time limit of the drift velocity ν as in the stationary state analysis. Therefore, we estimate the instantaneous mobility $\mu(t)$:

$$\mu(t) = \frac{\langle z(t + \Delta t/2) \rangle - \langle z(t - \Delta t/2) \rangle}{E \cdot \Delta t}, \quad (7)$$

the drift velocity is thus evaluated for a constant time lag Δt between the reference positions. We show in Figure S26 that for a sufficiently short time lag $\mu(t)$ does not depend on the choice of Δt . As a compromise between statistical noise and temporal resolution, we choose $\Delta t = 10$ ps for our following analysis.

The starting structures for this additional simulation set for the $r = 0.06$ system are extracted

from the $E_z = 0.0 \text{ V/nm}$ trajectory. The simulation procedure then consists of two steps: First, we freeze the polymer chains via harmonic restraints and simultaneously switch the field to $E_z = 1.0 \text{ V/nm}$. In this setting the ions may adjust to their local energy minima in an otherwise unchanged environment. Referring to our introductory sketch in Figure 1 this setting captures the plain tilting of the energy landscape. In the second step, the chains are released from the restraints and data is collected over a set of 100 individual simulations of 5 ns duration each. Further details on the simulation protocol are given in the Supplementary Information section S8.

In Figure 9 we show the time evolution of $R_{g,x/z}^2$ and the lithium coordination numbers after the polymer chains have been released from the restraints. We observe that for approximately 100 ps the structural quantities remain unchanged by the external field until they relax monotonously to their steady-state values within the simulation time window. Particularly the coordination numbers are at equilibrium after 1 ns. On that basis, we assume $\mu(t)$ to maintain μ_{dyn} until the structure starts transitioning and concurrently approach $\mu_{\text{dyn+struc}}$. We further emphasize that while $R_{g,x/z}^2$ quantifies structural changes on a mesoscopic level, the coordination numbers are a very local measure. Since both quantities respond with approximately the same delay of 100 ps to the external field, this suggests a typical time scale for other structural modifications.

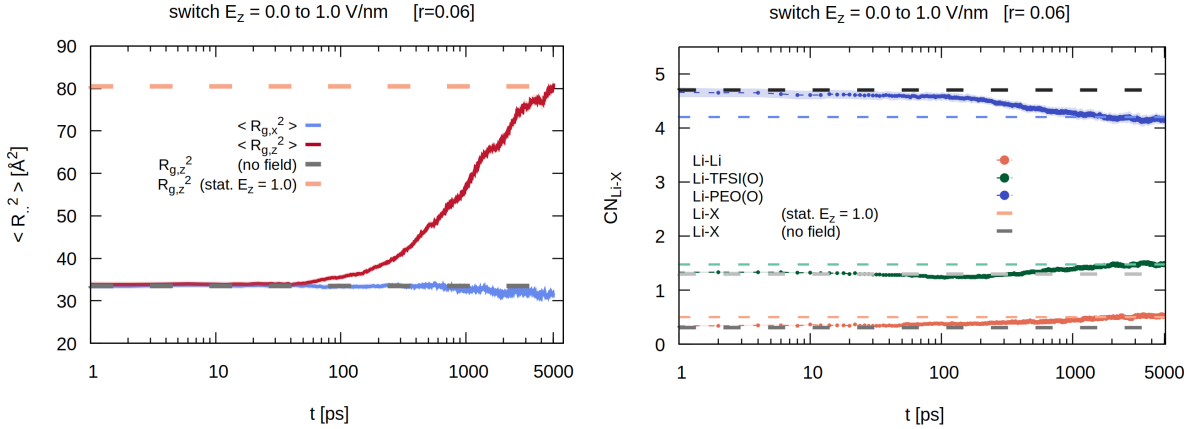


Figure 9: Time evolution of $R_{g,x}^2$ and $R_{g,z}^2$ (left) and lithium coordination environment (right) for field switched from $E_z = 0.0$ to 1.0 V/nm. The dashed lines correspond to the respective stationary state values.

The numerical results for $\mu(t)$ are shown in Figure 10. Indeed, we find that tilting the potential energy landscape effectuates an increase of the linear response μ_0 to $\mu_{\text{dyn}} \approx 4 \cdot \mu_0$. However, it is very unexpected that $\mu_{\text{dyn}} > \mu_{\text{dyn+struct}}$, thus $\mu(t)$ approaching its steady-state value from above. Interestingly, the polymer center of mass mobility μ_{PEO} is initially constant and then decreases to its steady-state value as well. We speculate the slowing μ_{PEO} to be a complex process beyond the scope of this work, possibly involving the observed structural alterations. Since lithium couples strongly to the polymer, we assume that the decrease of μ_{PEO} transfers on μ_{Li} , which is why we now consider $\mu_{\text{Li}}/\mu_{\text{PEO}}$. Figure 11 shows that the velocity of the lithium ions is initially twice as fast compared to the center of mass of the polymer chains and then decays exponentially to the steady-state ratio of $\mu_{\text{Li}}/\mu_{\text{PEO}} \approx 1.5$.

We attempt to understand the slowing down of the lithium dynamics qualitatively by means of a toy model. As discussed previously for the steady-state simulations under field application, the lithium ions pull the polymer chains into a stretched shape. Since such stretching reduces the number of possible chain conformations, i.e. the conformational entropy, the polymer responds to its decoiling with an elastic counter force comparable to an entropic spring.^{46–49}

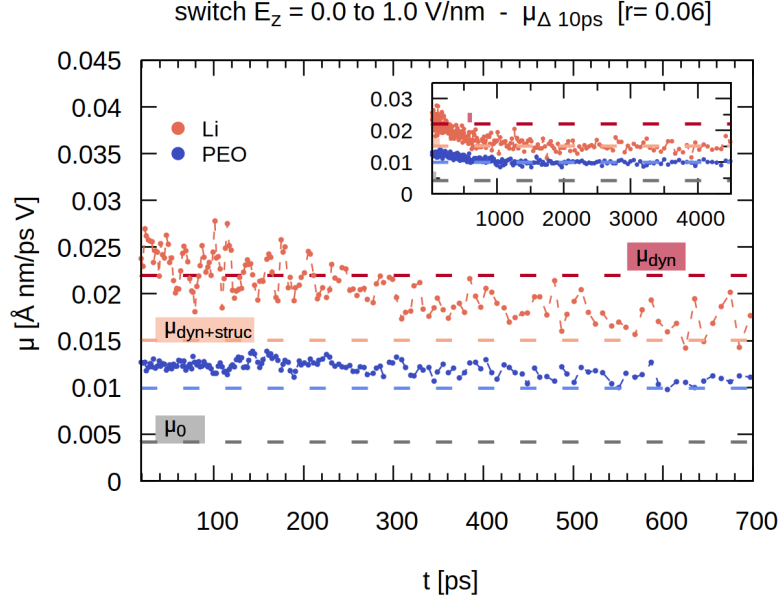


Figure 10: Instantaneous lithium and polymer (center of mass) mobilities calculated for a time lag of 10 ps (see Supplementary Information for further information) as a function of time since the field was switched from $E_z = 0.0$ to 1.0 V/nm. The dashed orange and blue horizontal lines correspond to the stationary state mobilities of lithium and polymer for $E_z = 1.0$ V/nm. The inset shows the long time behavior of μ_{Li} and μ_{PEO} .

In the idealized model, the lithium ion is portrayed as a particle attached to a spring, with the latter being representative of the polymer chain. The particle experiences an external pull F as well as an elastic back drag from the chain, scaling with the chain spring constant k . In the real case system the polymer chains are on average coordinated, and thus pulled, by multiple lithium ions, which is why we consider the tensile force acting on the polymer springs as an effective pull \tilde{F} . The overdamped dynamics of the particle position $x(t)$ and the center of mass of the spring $y(t)$ are described by a set of two differential equations:

$$\gamma_p \dot{x} = -k(x - y) + F \quad (8)$$

$$\gamma_s \dot{y} = \tilde{F}, \quad (9)$$

where γ_p and γ_s are the friction coefficients of particle and spring. Note that equation 9 is chosen in order to reproduce the basically constant PEO mobility directly after the switching.

Under the reasonable assumption of $x(0) = y(0)$, i.e. the particle and center of mass of the spring showing on average no initial displacement relative to each other, the solution yields:

$$x(t) = -\frac{\gamma_p}{k} \cdot \left(\frac{F}{\gamma_p} + \frac{\tilde{F}}{\gamma_s} \right) \exp\left(-\frac{k}{\gamma_p} t\right) + \frac{\tilde{F}}{\gamma_s} \cdot t + \frac{\gamma_p}{k} \cdot \left(\frac{F}{\gamma_p} + \frac{\tilde{F}}{\gamma_s} \right) \quad (10)$$

$$y(t) = \frac{\tilde{F}}{\gamma_s} \cdot t. \quad (11)$$

Whereas the center of mass of the spring displays a uniform motion at a steady velocity of $v_\infty = \tilde{F}/\gamma_s$, the particle dynamics relax exponentially to v_∞ . In other words, the particle initially migrates faster than the spring until its motion is increasingly restrained by the thereby elongated spring:

$$\frac{\mu_{\text{Li}}(t)}{\mu_{\text{spring}}(t)} \propto \frac{\dot{x}(t)}{\dot{y}(t)} = 1 + A \cdot \exp(-Bt), \quad (12)$$

where $A = \left(\frac{F\gamma_s}{\tilde{F}\gamma_p} + 1 \right)$ and $B = \frac{k}{\gamma_p}$. However, in the real case system the lithium ion is bound to the polymer chain for a mean residence time τ only before it hops into a new coordination environment, for example a different polymer chain. Such events serve as a renewal process for the lithium dynamics, which then become uncorrelated to their past. While we know from the steady-state simulations at $E_z = 0.0 \text{ V/nm}$ and $E_z = 1.0 \text{ V/nm}$ that the residence times drop from over 260 ns to 2.8 ns, we observe a significant amount of exchange events before 3 ns have passed after the field switch as shown in Figure S27.

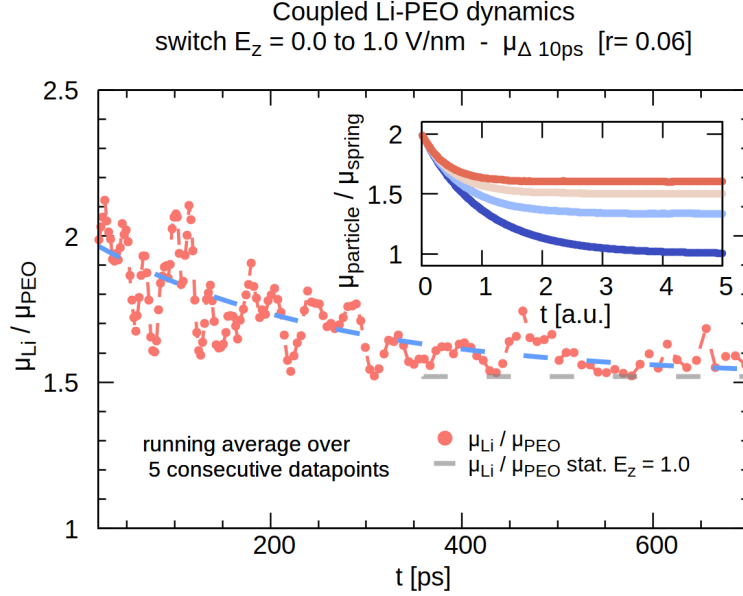


Figure 11: Ratio of lithium and polymer mobilities as a function of time since the field was switched from $E_z = 0.0$ to 1.0 V/nm. The dashed line shows qualitatively the exponential decay $(\mu_{\text{Li}}(t)/\mu_{\text{PEO}}(t) = \alpha \cdot \exp(-t/\beta) + \gamma$ with $\alpha = 0.49$, $\beta = 249$ ps and $\gamma = \lim_{t \rightarrow \infty} \mu_{\text{Li}}(t)/\mu_{\text{PEO}}(t) = 1.52$) fitted as a guide to the eye.

The inset shows the mobility ratios for the simplified particle-spring-model set up by equations (8) and (9), which has been solved. The dark blue curve corresponds to the expected ratio of 1 if no particle-spring-exchange events are considered. For increasing exchange rates, i.e. shorter residence time of a particle on a spring, the condition $x = y$ is renewed with a rate Γ and the long-time plateau shifts to higher values.

We now demonstrate how incorporation of such hopping events, which occur at a rate Γ , cause an upshift of the particle velocity at long times. Assuming that the lithium particles hop onto a new polymer spring at a rate Γ , the condition $x = y$ is on average renewed at a rate Γ as well. For an exponentially distributed residence time on the chain

$P_{\Gamma} = \Gamma \cdot \exp(-\Gamma t)$,⁵⁰ the long-time plateau for the ratio of particle and spring velocities gets an additional contribution as displayed in the inset in Figure 11:

$$\lim_{t \rightarrow \infty} \frac{\mu_{\text{Li}}(t)}{\mu_{\text{spring}}(t)} = 1 + \int_0^{\infty} dt A \cdot \exp(-Bt) \cdot \Gamma \exp(-\Gamma t) = 1 + \frac{A\Gamma}{B + \Gamma}. \quad (13)$$

Vividly speaking, the minimal model provides us with the qualitative conception that

the motion of the individual lithium ions is held back by an entropic penalty arising from the chain stretching as sketched in Figure 12. Yet, the lithium ions exchange the polymer chains and may initially, i.e. after hopping onto a new chain, migrate at a speed faster than the center of mass of the chain they are bound to.

We gather further evidence supporting this interpretation from analyzing $\Delta z_{\text{Li-PEO}}$, the displacement of lithium relative to the center of mass of the chain that the lithium ion is attached to, as a function of the time since the field has been switched on.

To meet the assumptions upon which the idealized toy model is based as close as possible, we discuss $\Delta z_{\text{Li-PEO}}(t)$ for the subensemble of special lithium-chain pairs that exist since $t = 0$ ps and, secondly, for which the chain is coordinated via a single lithium ion only and the lithium ion in return is bound exclusively to this chain as well. As shown in Figure 13 the drift of the lithium ions is sublinear in the reference frame of its coordinating polymer with $\Delta z_{\text{Li-PEO}}(t) \propto t^{0.7}$ at short times, which is indicative of the restraining effect of the polymer chain.

Whereas initially $\Delta z_{\text{Li-PEO}}(0) = 0$ holds, the relative shift plateaus at long times which means that the forces acting on the lithium ion must balance, i.e. lithium pulling the polymer chain in field direction and concurrently experiencing a counter force originating from the thereby stretched chain.

We note that according to Rouse theory, and due to the strong coupling of lithium and polymer segmental dynamics, a scaling of $\Delta z_{m\text{-com}}(t) \propto \sqrt{t}$ is predicted analytically for an arbitrary monomer m , that is being pulled by an external force, relative to the center of mass of the chain. We assume that the deviation of the scaling exponent may be related to the onset of structural modifications of the polymer, which is no longer covered by the Rouse model.

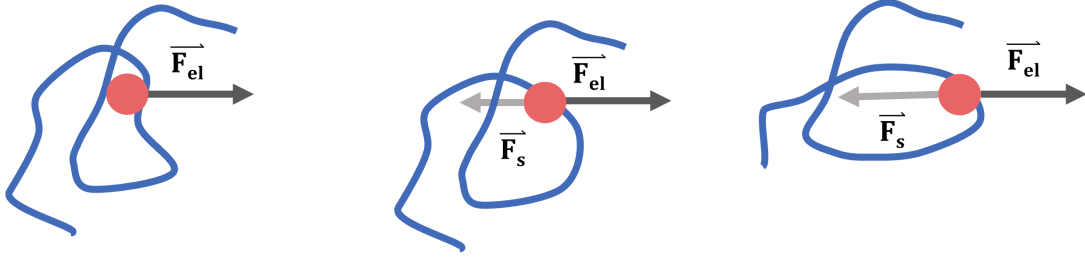


Figure 12: Sketch of electric field and polymer chain exerting an electric force \vec{F}_{el} , respectively entropic force \vec{F}_s on lithium.

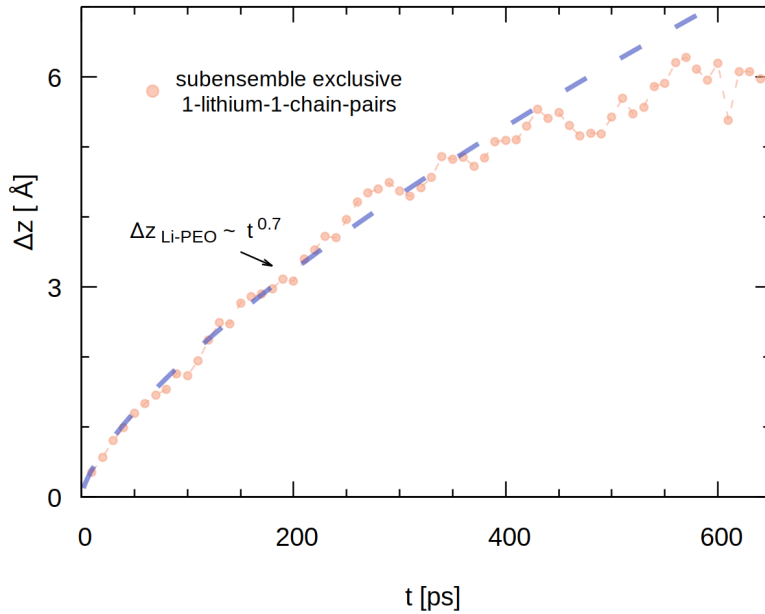


Figure 13: Time evolution of lithium displacement relative to the center of mass of the polymer chain, that it is attached to, Δz_{Li-PEO} for the subensemble of distinct lithium-chain-pairs existent at $t = 0$ ps, where lithium coordinates to a single chain and the chain is coordinated exclusively by this lithium ion.

Conclusion We have performed an extensive all-atomistic molecular dynamics simulation study on the impact of external electric fields (0-1 V/nm) on structural and transport properties in polymer electrolyte systems. Motivated by recent experimental findings on nonlinear dynamics in PEO/LiTFSI electrolytes and arising speculations on field-induced ordering of the polymer host matrix that facilitates ion motion,¹⁹ our aim was to understand the correlation of field effects (if any) between structure and ion dynamics.

We found strong nonlinearities of the transport properties μ and D_{\parallel} whose origin can be attributed to a tilt of the potential energy surface in field direction and, possibly, to an additional decrease of the activation barriers due to structural changes.

We observed significant structural alterations of the lithium coordination environment and polymer chain elongation in the presence of an electric field. We found that the lithium ions are progressively liberated from the polymer backbone, and furthermore that an asymmetric attachment of lithium to the chain causes a stretching of the polymer in direction of the field. This could be interpreted as a tentative indicator of the aforementioned channel structures.

To discuss the nonlinear effects for both structural and dynamical observables in a common framework, we defined a critical field strength E_c that quantifies the field susceptibility of the observable. The results suggest a weak influence of the structural changes on the enhancement of the dynamics because the field strengths necessary to change the structure are either significantly higher than $E_{c,dyn}$, or they display the opposite dependence on salt concentration. Furthermore, we recall the observation that the structural field dependence of the chain elongation levels off for fields approaching 1 V/nm whereas no such saturation is observed for the dynamical properties.

Since it cannot be excluded that already minor modification of a yet not discussed structural observable provokes a dramatic reduction of the activation barriers, the causality issue remained unresolved to this point. Therefore, we employed non-equilibrium simulations and monitored the temporal evolution of structure and dynamics in response to an external field. Starting from an $E_z = 0.0$ V/nm configuration we switched to $E_z = 1.0$ V/nm and observed that μ is, counterintuitively, slowed down. We were able to present a microscopic understanding for this behavior and conclude on the question of causality: The nonlinear enhancement of the lithium dynamics owes to the tilting of the energy landscape in direction of the external field. Because the lithium ions pull the polymer into a stretched shape, thereby reducing the conformational entropy of the chains, the lithium dynamics decelerate.

Within this theoretical framework we might also give an answer to the opposed concentration dependencies for chain structure measured via $R_{g,z}^2$ on the one hand, and the lithium transport properties μ and $D_{||}$ on the other. Because an increasing chain stretching implies a higher entropic penalty, the dynamics are increasingly impeded for decreasing salt content, which has been previously found to allow for a higher ordering of the polymer host. Hence, we are able to give evidence, quite surprisingly, on an adverse net effect of the structural ordering on the dynamics, that means causing a slowing down.

Referring to the uncertain origin of the field-induced transport enhancement which was observed in eNMR measurements, performed at electric field strengths five orders of magnitude below the field strengths where our simulation study reveals nonlinear contributions,¹⁹ we suggest that the eNMR can be rather explained by bulk flow effects, as already given as an alternative explanation in that work.

We hope that our findings on the rich dynamical behavior of lithium in a polymer electrolyte system draw attention to the nonlinear effects, which may emerge in the close environment of charged interfaces, i.e. the vicinity of electrodes where even minor drops of the electric potential can result in high fields.

Acknowledgement

Analysis and simulations have been performed on the computing cluster PALMA2 at the University of Münster. We thankfully acknowledge the financial support from MWIDE NRW as part of the "GrEEEn" project (funding code: 313-W044A) and the Federal Ministry of Education and Research (BMBF) for funding within the FestBatt cluster (funding number 03XP0174B).

Supporting Information Available

Simulation procedure, velocity distributions, coordination numbers (Li-Li, Li-TFSI(O)), PEO-monomer dipole angle distributions, μ_{TFSI} , $R_{\text{g},z}^2$ for ions subjected to the external field only, pull-stretching-mechanism and s_{asym} statistics, comparison of $R_{\text{g},z}^2$, μ and D_{parallel} for longer polymer chains, $\mu_{\text{Li}}(t)$ for switching E_z , $\tau_{\text{Li-PEO chain}}$, $\Delta\tilde{z}_{\text{Li-PEO}}$ analysis including all lithium-chain pairs.

References

- (1) Tarascon, J.-M. Key challenges in future Li-battery research. *Philosophical Transactions of the Royal Society A: Mathematical, Physical and Engineering Sciences* **2010**, *368*, 3227–3241.
- (2) Scrosati, B.; Garche, J. Lithium batteries: Status, prospects and future. *Journal of Power Sources* **2010**, *195*, 2419–2430.
- (3) Tarascon, J.-M.; Armand, M. Issues and challenges facing rechargeable lithium batteries. *Nature* **2001**, *414*, 359–367.
- (4) Xu, K. Nonaqueous Liquid Electrolytes for Lithium-Based Rechargeable Batteries. *Chemical reviews* **2004**, *104*, 4303–4418.
- (5) Armand, M. B. Polymer electrolytes. *Annual Review of Materials Science* **1986**, *16*, 245–261.
- (6) Bruce, P. G.; Vincent, C. A. Polymer electrolytes. *Journal of the Chemical Society, Faraday Transactions* **1993**, *89*, 3187.
- (7) Fenton, D.; Parker, J.; Wright, P. Complexes of alkali metal ions with poly(ethylene oxide). *Polymer* **1973**, *14*, 589.

- (8) Quartarone, E.; Mustarelli, P.; Magistris, A. PEO-based composite polymer electrolytes. *Solid State Ionics* **1998**, *110*, 1–14.
- (9) Gadjourova, Z.; Andreev, Y. G.; Tunstall, D. P.; Bruce, P. G. Ionic conductivity in crystalline polymer electrolytes. *Nature* **2001**, *412*, 520–523.
- (10) Xu, K. Electrolytes and interphases in Li-ion batteries and beyond. *Chemical reviews* **2014**, *114*, 11503–11618.
- (11) Manuel Stephan, A.; Nahm, K. Review on composite polymer electrolytes for lithium batteries. *Polymer* **2006**, *47*, 5952–5964.
- (12) Jorn, R.; Kumar, R.; Abraham, D.; Voth, G. Atomistic Modeling of the Electrode-Electrolyte Interface in Li-Ion Energy Storage Systems: Electrolyte Structuring. *The Journal of Physical Chemistry C* **2013**, *117*, 3747–3761.
- (13) Matse, M.; Berg, P.; Eikerling, M. Asymmetric double-layer charging in a cylindrical nanopore under closed confinement . *The Journal of Chemical Physics* **2020**, *152*.
- (14) Kreuzer, H. Physics and chemistry in high electric fields. *Surface and Interface Analysis* **2002**, *36*, 372–379.
- (15) Stuve, E. Ionization of water in interfacial electric fields: An electrochemical view. *Chemical Physics Letters* **2012**, *519-520*, 1–17.
- (16) Harry, K.; Hallinan, D.; Parkinson, D.; MacDowell, A.; Balsara, N. Detection of subsurface structures underneath dendrites formed on cycled lithium metal electrodes. *Nature Materials* **2014**, *13*, 69–73.
- (17) Jaeckle, M.; Gross, A. Influence of electric fields on metal self-diffusion barriers and its consequences on dendrite growth in batteries. *The Journal of Chemical Physics* **2019**, *151*, 234707.

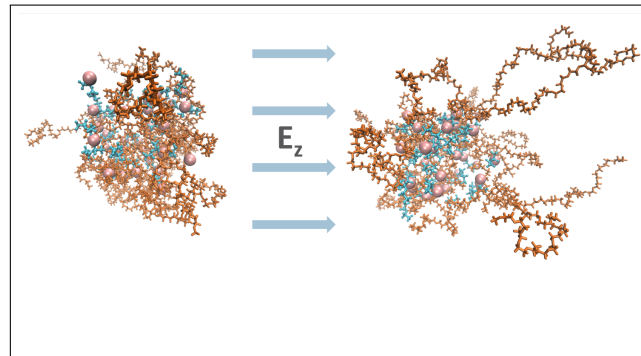
- (18) Linlin, L.; Siyuan, L.; Yingying, L. Suppression of dendritic lithium growth in lithium metal-based batteries. *Chemical Communications* **2018**, *54*, 6648–6661.
- (19) Rosenwinkel, M. P.; Schönhoff, M. Lithium Transference Numbers in PEO/LiTFSa Electrolytes Determined by Electrophoretic NMR. *Journal of The Electrochemical Society* **2019**, *166*, A1977–A1983.
- (20) Wang, J.; Lei, J. Influence of DC electric field on both crystalline structure and conductivity of poly(ethylene oxide)10:LiClO₄ electrolyte. *Journal of Polymer Science Part B: Polymer Physics* **2012**, *50*, 656–667.
- (21) Sunitha V. R., S. V.; Radhakrishnan S., R. Field enhanced Li ion conduction in nano-ferroelectric modified polymer electrolyte systems. *Ionics* **2015**, *21*, 949–954.
- (22) Huang, Y.; Jämbeck, J.; Unge, M. Understanding the Ionic Conduction in Dielectric Polymers at High Electric Fields Using Molecular Dynamics Simulations. *ACS Macro Letters* **2017**, *6*, 571–574.
- (23) Heuer, A.; Schroer, C. F. E.; Diddens, D.; Rehwald, C.; Blank-Burian, M. Nonlinear response from the perspective of energy landscapes and beyond. *The European Physical Journal Special Topics* **2017**, *226*, 3061–3078.
- (24) Kunow, M.; Heuer, A. Nonlinear ionic conductivity of lithium silicate glass studied via molecular dynamics simulations. *The Journal of Chemical Physics* **2006**, *124*, 214703.
- (25) Schroer, C. F. E.; Heuer, A. Understanding the nonlinear dynamics of driven particles in supercooled liquids in terms of an effective temperature. *The Journal of Chemical Physics* **2015**, *143*, 224501.
- (26) Roling, B.; Murugavel, S.; Heuer, A.; Lühning, L.; Friedrich, R.; Röthel, S. Field-dependent ion transport in disordered solid electrolytes. *Physical Chemistry Chemical Physics* **2008**, *10*, 4211.

- (27) Genreith-Schriever, A. R.; De Souza, R. A. Field-enhanced ion transport in solids: Reexamination with molecular dynamics simulations. *Physical Review B* **2016**, *94*, 224304.
- (28) Berendsen, H. J.; van der Spoel, D.; van Drunen, R. GROMACS: A message-passing parallel molecular dynamics implementation. *Computer Physics Communications* **1995**, *91*, 43–56.
- (29) Van Der Spoel, D.; Lindahl, E.; Hess, B.; Groenhof, G.; Mark, A. E.; Berendsen, H. J. GROMACS: Fast, flexible, and free. *Journal of Computational Chemistry* **2005**, *26*, 1701–1718.
- (30) Páll, S.; Abraham, M. J.; Kutzner, C.; Hess, B.; Lindahl, E. Tackling exascale software challenges in molecular dynamics simulations with GROMACS. Lecture Notes in Computer Science (including subseries Lecture Notes in Artificial Intelligence and Lecture Notes in Bioinformatics). 2015; pp 3–27.
- (31) Abraham, M. J.; Murtola, T.; Schulz, R.; Páll, S.; Smith, J. C.; Hess, B.; Lindahl, E. Gromacs: High performance molecular simulations through multi-level parallelism from laptops to supercomputers. *SoftwareX* **2015**, *1-2*, 19–25.
- (32) Jorgensen, W. L.; Maxwell, D. S.; Tirado-Rives, J. Development and testing of the OPLS all-atom force field on conformational energetics and properties of organic liquids. *Journal of the American Chemical Society* **1996**, *118*, 11225–11236.
- (33) Canongia Lopes, J. N.; Padua, A. A. CL&P: A generic and systematic force field for ionic liquids modeling. *Theoretical Chemistry Accounts* **2012**, *131*, 1–11.
- (34) Lopes, J. N.; Padua, A. A. Molecular force field for ionic liquids composed of triflate or bistriflylimide anions. *Journal of Physical Chemistry B* **2004**, *108*, 16893–16898.

- (35) Canongia Lopes, J. N.; Deschamps, J.; Padua, A. A. H. Modeling Ionic Liquids Using a Systematic All-Atom Force Field. *The Journal of Physical Chemistry B* **2004**, *108*, 2038–2047.
- (36) Shimizu, K.; Almantariotis, D.; Costa Gomes, M. F.; Pádua, A. A.; Canongia Lopes, J. N. Molecular force field for ionic liquids V: Hydroxyethylimidazolium, dimethoxy-2methylimidazolium, and fluoroalkylimidazolium cations and Bis(fluorosulfonyl)amide, perfluoroalkanesulfonylamide, and fluoroalkylfluorophosphate anions. *Journal of Physical Chemistry B* **2010**, *114*, 3592–3600.
- (37) Heuer, A.; Murugavel, S.; Roling, B. Nonlinear ionic conductivity of thin solid electrolyte samples: Comparison between theory and experiment. *Physical Review B* **2005**, *72*, 174304.
- (38) Blickle, V.; Speck, T.; Lutz, C.; Seifert, U.; Bechinger, C. Einstein Relation Generalized to Nonequilibrium. *Physical Review Letters* **2007**, *98*, 210601.
- (39) Borodin, O.; Smith, G. D. Mechanism of Ion Transport in Amorphous Poly(ethylene oxide)/LiTFSI from Molecular Dynamics Simulations. *Macromolecules* **2006**, *39*, 1620–1629.
- (40) Brooks, D. J.; Merinov, B.; Goddard, W.; Kozinsky, B.; Mailoa, J. Atomistic Description of Ionic Diffusion in PEO/LiTFSI: Effect of Temperature, Molecular Weight, and Ionic Concentration. *Macromolecules* **2018**, *51*, 8987–8995.
- (41) Timachova, K.; Watanabe, H.; Balsara, N. Effect of Molecular Weight and Salt Concentration on Ion Transport and the Transference Number in Polymer Electrolytes. *Macromolecules* **2015**, *48*, 7882–7888.
- (42) Costa, L. T.; Sun, B.; Jeschull, F.; Brandell, D. Polymer-ionic liquid ternary systems for Li-battery electrolytes: Molecular dynamics studies of LiTFSI in a EMIm-TFSI and PEO blend. *Journal of Chemical Physics* **2015**, *143*, 024904.

- (43) Diddens, D.; Heuer, A. Simulation Study of the Lithium Ion Transport Mechanism in Ternary Polymer Electrolytes: The Critical Role of the Segmental Mobility. *The Journal of Physical Chemistry B* **2014**, *118*, 1113–1125.
- (44) Molinari, N.; Mailoa, J. P.; Kozinsky, B. Effect of Salt Concentration on Ion Clustering and Transport in Polymer Solid Electrolytes: A Molecular Dynamics Study of PEO-LiTFSI. *Chemistry of Materials* **2018**, *30*, 6298–6306.
- (45) Müller-Plathe, F.; van Gunsteren, W. F. Computer simulation of a polymer electrolyte: Lithium iodide in amorphous poly(ethylene oxide). *The Journal of Chemical Physics* **1995**, *103*, 4745–4756.
- (46) Doi, M.; Edwards, S. F.; Edwards, S. F. *The theory of polymer dynamics*; oxford university press, 1988; Vol. 73.
- (47) Ortiz, C.; Hadziioannou, G. Entropic elasticity of single polymer chains of poly(methacrylic acid) measured by atomic force microscopy. *Macromolecules* **1999**, *32*, 780–787.
- (48) Strobl, G. R.; Strobl, G. R. *The physics of polymers*; Springer, 1997; Vol. 2.
- (49) Liese, S.; Gensler, M.; Krysiak, S.; Schwarzl, R.; Achazi, A.; Paulus, B.; Hugel, T.; Rabe, J. P.; Netz, R. R. Hydration effects turn a highly stretched polymer from an entropic into an energetic spring. *ACS nano* **2017**, *11*, 702–712.
- (50) Diddens, D.; Heuer, A. Lithium ion transport mechanism in ternary polymer electrolyte-ionic liquid mixtures: A molecular dynamics simulation study. *ACS Macro Letters* **2013**, *2*, 322–326.

Graphical TOC Entry



Supplementary Information:

Polymer electrolytes in strong external electric fields: Modification of structure and dynamics

Alina Wettstein,^{*,†} Diddo Diddens,[‡] and Andreas Heuer^{*,‡,†}

[†]*Institut für physikalische Chemie, Westfälische Wilhelms-Universität Münster, Corrensstraße 28/30,
D-48149 Münster, Germany*

[‡]*Institut für Energie- und Klimaforschung, Ionics in Energy Storage, Helmholtz Institut Münster,
Forschungszentrum Jülich, Corrensstraße 46, 48149 Münster, Germany*

E-mail: alina.wettstein@gmail.com; andheuer@wwu.de

S1: Simulation procedure

The simulation study presented in this work was carried out by means of the molecular dynamics (MD) software package GROMACS (version 2018.6).¹⁻⁴ The force field parameters for poly(ethylene oxide) (PEO) rely on the classic all-atom, non-polarizable OPLS-AA force field,⁵ whereas the Li[TFSI] interactions were parameterized by the widely acknowledged OPLS-AA-based CL&P force field developed by Canongia Lopes and Padua.⁶⁻⁹ To account for the neglected polarizability, which entails effective charge screening and transfer,¹⁰⁻¹⁵ in a mean field sense, all partial atom point charges were uniformly rescaled by a factor of 0.8 according to prevalent practice.¹⁶⁻²³ While other simulation studies urgently promote to employ polarizable force field models,^{24,25} the gained accuracy in defining the atomistic local environment comes at the expense of computational effort and feasible simulation times, which are required to be sufficiently long to sample the diffusive regime of the particle dynamics for this research purpose.

If not stated otherwise, all molecular dynamics simulations were performed according to the following protocol. The initial configurations were generated in the gas phase at a temperature of 423 K with the Packmol package,²⁶ where both the lithium salt and coiled PEO chains, as they exist in the molten state, were randomly distributed in a cubic box. After an energy minimization the system was shrunk under NPT conditions for 2.5 ns using a high coupling constant of 2 ps to a Berendsen barostat with a reference pressure of 1 bar at a small integration time step of 0.5 fs (Berendsen thermostat, $\tau_T = 1$ ps). To ensure a well relaxed configuration the system was further equilibrated for 200 ns with a step size of 2 fs in a constant NPT ensemble, where pressure and temperature were controlled by a Berendsen barostat and a velocity-rescale thermostat.^{27,28} Moreover, the linear constraint solver (LINCS) was used to constrain the hydrogen bonds.^{29,30} Taking the hence equilibrated system as a starting structure, a constant external electric field oriented in z -direction was switched on and the system was further propagated for 90 ns, before beginning data acquisition in a productive simulation run in a constant NPT ensemble, whereas here pressure and temperature couple to an extended Parrinello-Rahman and Nose-Hoover ensemble.³¹⁻³⁴ In order to reach the diffusive regime of the lithium ions and ensure sufficient sampling, the duration of the productive runs extends up to 2 μ s, but covers at least 300 ns. The center of mass of the system was repositioned every 10th simulation step.

We further present exemplary velocity distribution profiles for the lithium ions parallel and perpendicular to the external electric field (see Figures 1 and 2) to ensure correct sampling of the Maxwell-Boltzmann distribution. Computing the non-gaussianity parameter $\alpha = 1/3 \cdot \langle v_i^4 \rangle / \langle v_i^2 \rangle^2 - 1$, i.e. the ratio of second and fourth moments of the instant velocity distribution in each dimension i , which would vanish for a truly Gaussian distribution, α_{para} and α_{ortho} yields values in the order of $10^{-2} \approx 0$.

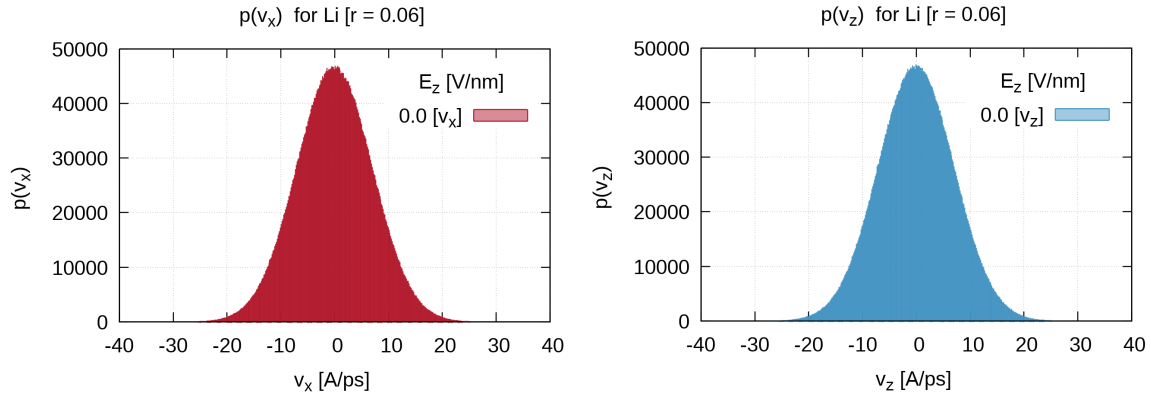


Figure S1: Histogram of lithium velocities in arbitrary directions in absence of an external field.

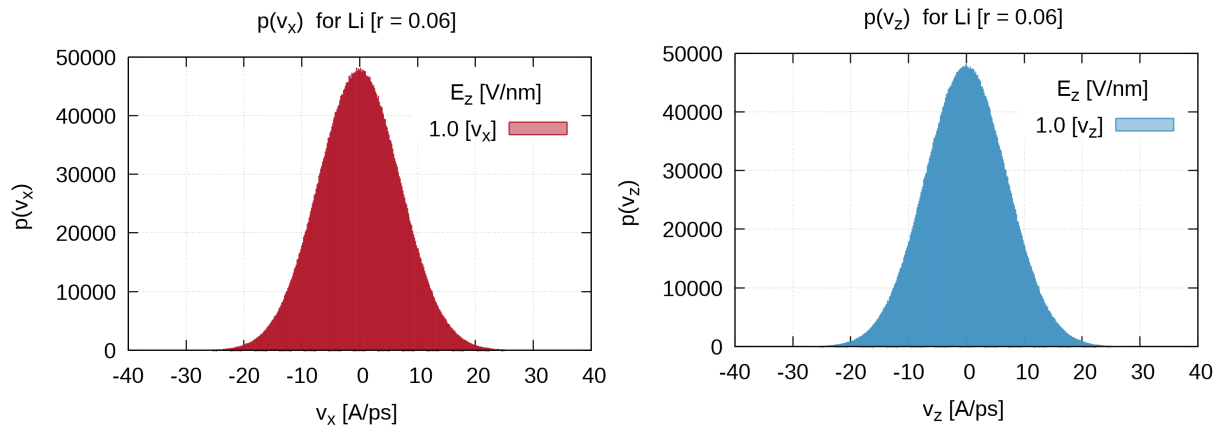


Figure S2: Histogram of lithium velocities in x and z -direction for application of an external field strength of 1.0 V/nm in z -direction.

S2: Dynamic response TFSI and lithium-chain mean residence times

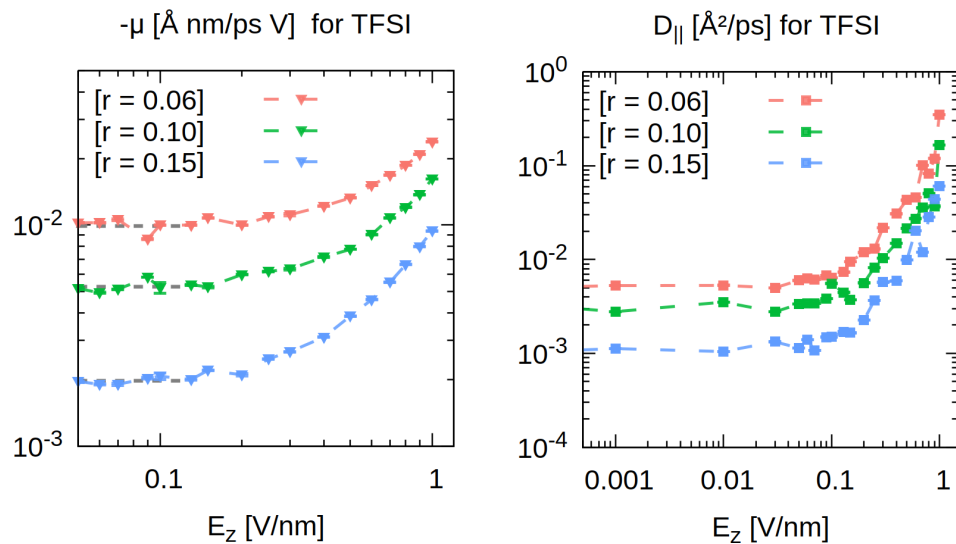


Figure S3: TFSI mobilities μ and parallel diffusion constants D_{\parallel} as a function of electric field strength for three different salt concentrations.

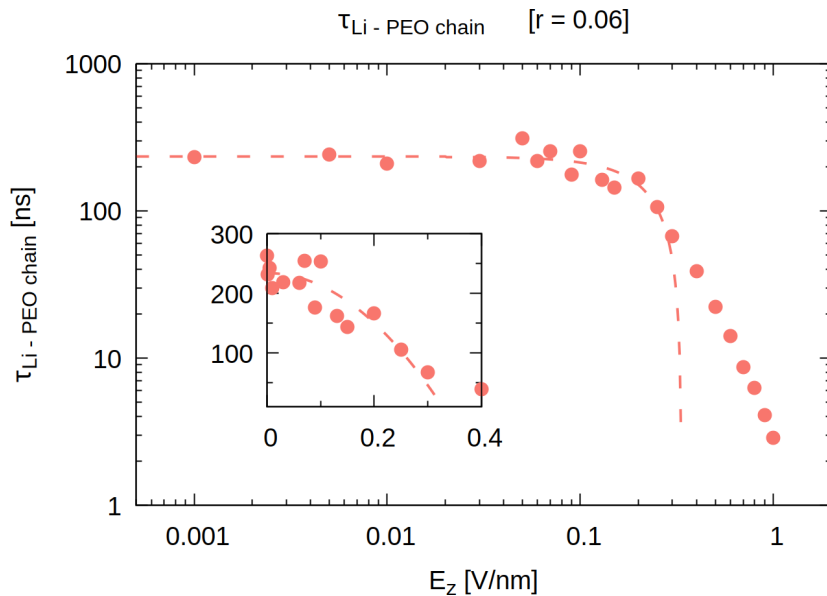


Figure S4: Mean residence time of lithium on polymer chain as a function of E_z for $r = 0.06$ and example quadratic E_c fit ($E_c = 0.33$ V/nm).

S3: RDF and cumulative numbers

For the highest salt content the average lithium coordination cage is composed of two TFSI anion oxygens and four ether oxygens in absence of an electric field, which is in excellent accordance with literature values for similar salt concentration.^{17,35} For lower salt contents the lithium-ether-oxygen coordination is higher, which may be attributed to a mere excess supply of vacant polymer segments.¹⁷

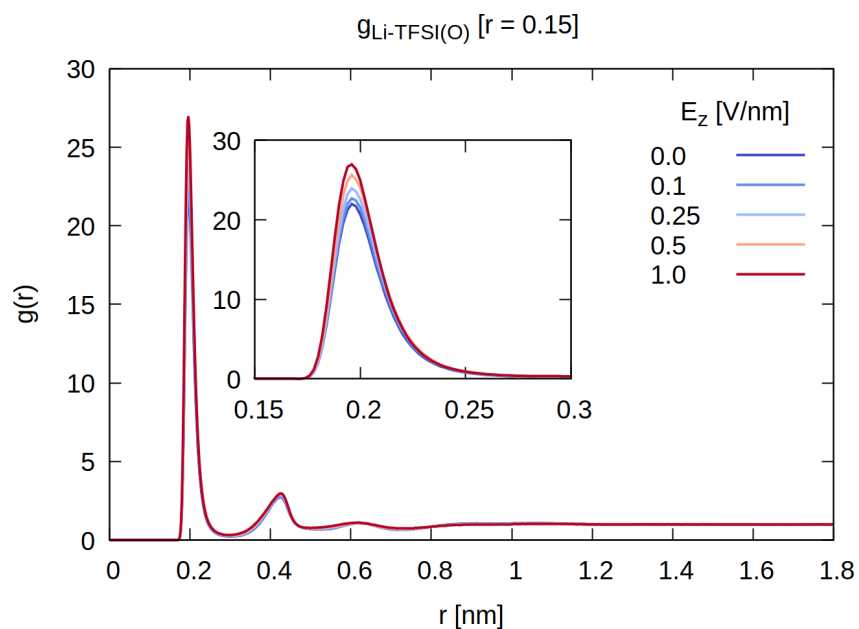


Figure S5: Exemplary lithium-TFSI(O) radial distribution functions as a function of electric field strength for the $r = 0.15$ electrolyte mixture.

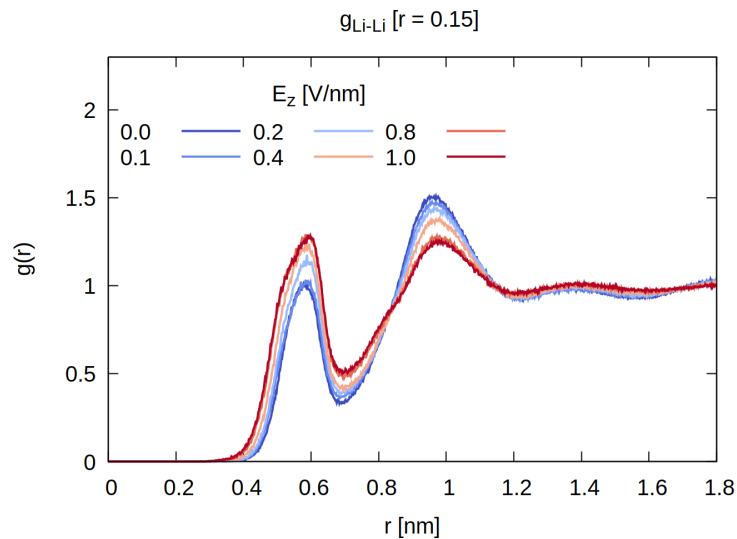


Figure S6: Exemplary lithium-lithium radial distribution functions as a function of electric field strength for the $r = 0.15$ electrolyte mixture.

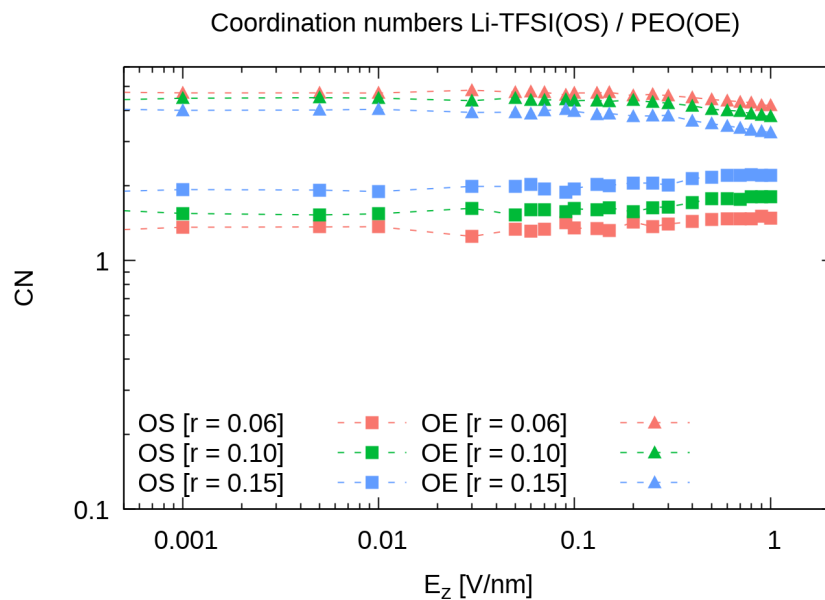


Figure S7: Electric field dependence of the Li - OS(TFSI) and Li - OE(PEO) coordination numbers for various salt concentrations.

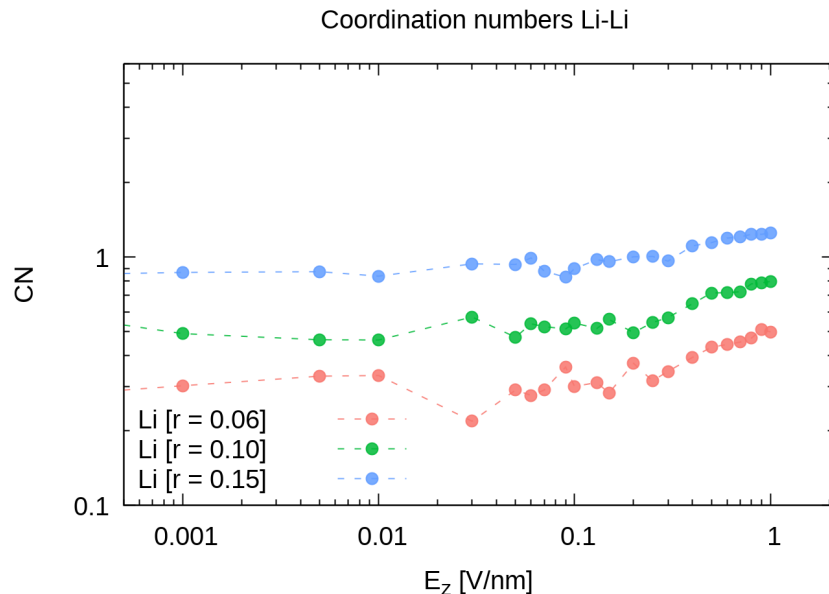


Figure S8: Li-Li coordination numbers as a function of electric field strength for different salt contents.

Table S1: Relative frequencies of chain coordination motifs in absence of electric field and a maximum electric field strength of $E_z = 1.0$ V/nm for various salt concentrations. The label 'free' means that lithium is not coordinated by the polymer.

| $r = [\text{Li}]/[\text{EO}]$ | free [%] | | 1 chain [%] | | 2 chains [%] | |
|-------------------------------|----------|------------|-------------|------------|--------------|------------|
| | 0.0 | 1.0 [V/nm] | 0.0 | 1.0 [V/nm] | 0.0 | 1.0 [V/nm] |
| 0.06 | 0.5 | 3.0 | 96.9 | 81.3 | 2.6 | 15.7 |
| 0.10 | 5.1 | 6.7 | 93.7 | 82.6 | 1.2 | 10.7 |
| 0.15 | 5.7 | 13.6 | 93.6 | 79.2 | 0.7 | 7.2 |

S4: Monomer dipole orientation

As mentioned in the main text we observe a deceleration of the polymer ordering captured via $R_{g,z}^2$ for electric field strengths above 0.6 V/nm. To understand this behavior we study the orientation of the local monomer dipoles \vec{p}_{mon} , constituted by the partially charged C-O-C segments, relative to the external field. The probability distribution of the angle between two randomly pointing vectors is proportional to $\sin(\varphi)$. We choose φ as $\angle(\vec{E}_z, \vec{p}_{\text{mon}})$. As shown in Figures S9 and S11 we recover the expected sinusoidal distribution in the plain

polymer as well as the $r = 0.06$ electrolyte mixture in absence of an external field when the structure of the polymer host has not received an orientation. For application of an external field we observe a shift of φ to smaller angles which means that individual monomer dipoles increasingly point in field direction. This local dipole \vec{p}_{mon} alignment in field direction corresponds to an orientation of the C-O-C segment perpendicular to the field. Hence, the polymer chains contract and counteract the overall alignment in the field. To further assess the intensity of this effect, we normalize the distributions of φ to φ_0 when no field is applied. As shown in Figure S12 the effect is less pronounced for the salt-in-polymer electrolyte.

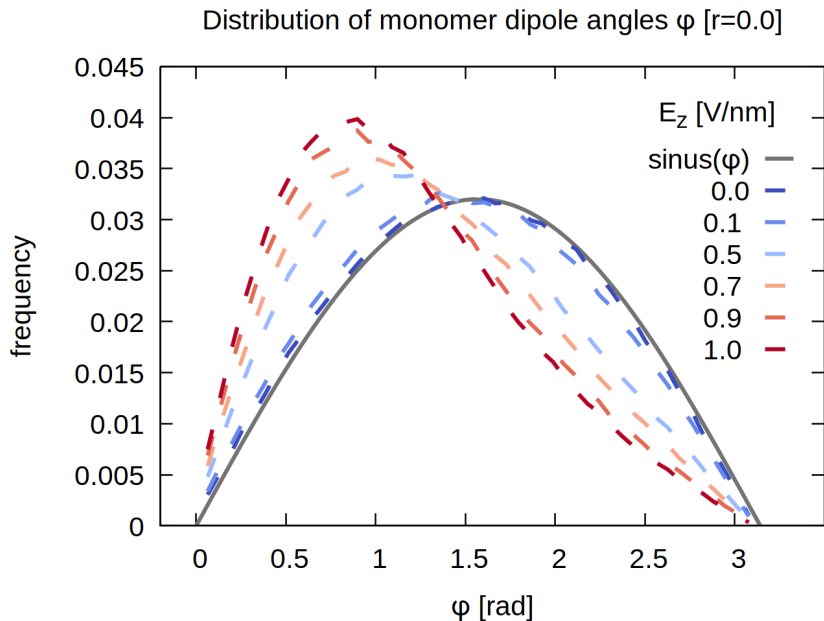


Figure S9: Probability distribution of the angles of the individual monomer dipole C-O-C sections relative to field orientation in the plain polymer system for various electric field strengths.

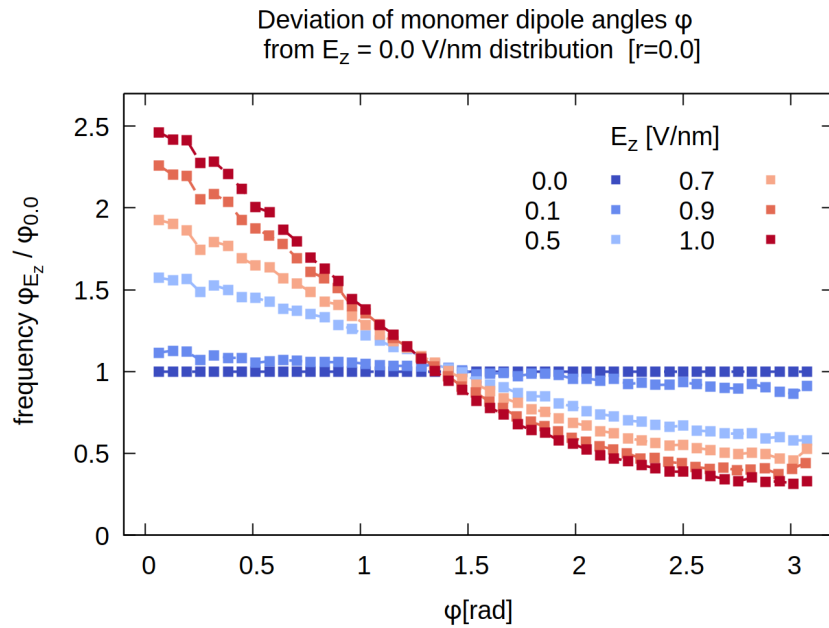


Figure S10: Deviation of probability distribution in Figure S9 from field-free reference $\varphi_{0,r=0.0}$.

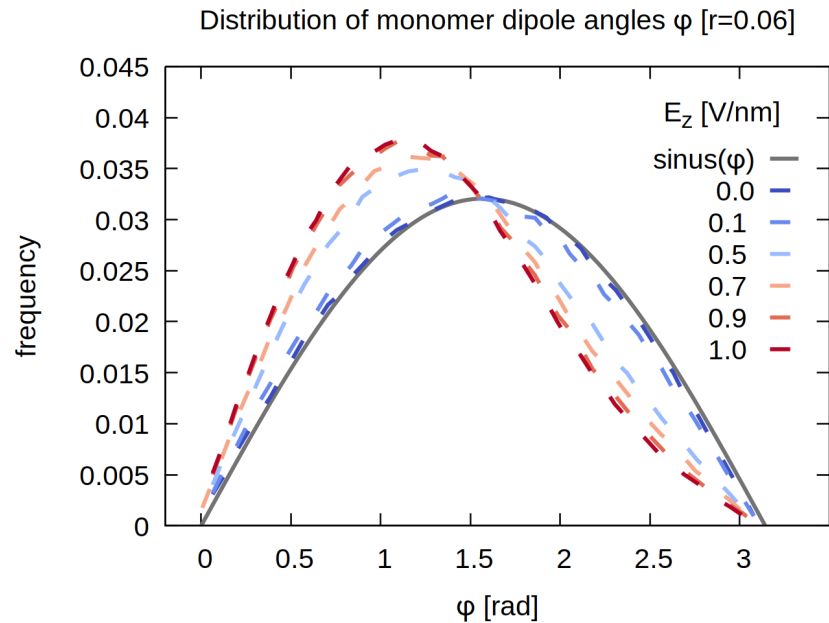


Figure S11: Probability distribution of the angles of the individual monomer dipole C-O-C sections relative to field orientation in the $r = 0.6$ salt-in-polymer mixture for various electric field strengths.

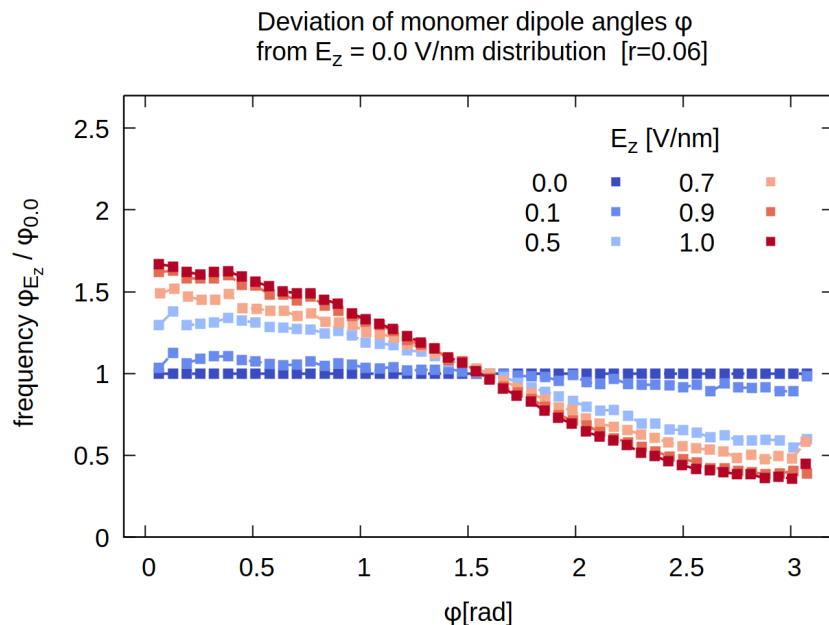


Figure S12: Deviation of probability distribution in Figure S11 from field-free reference $\varphi_{0,r=0.06}$.

S5: Comparison $R_{g,z}^2$ for electric field applied on ions only

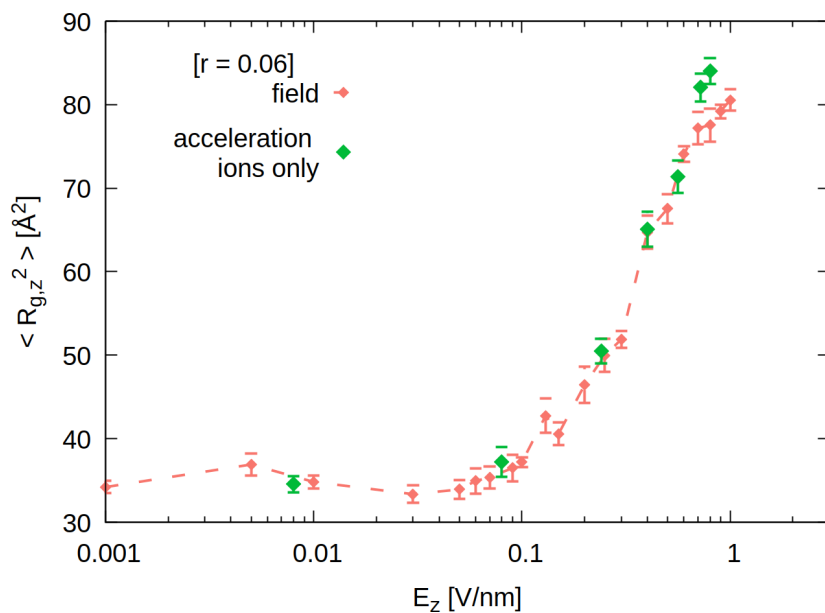


Figure S13: Comparison of gyration radii $R_{g,z}^2$ for the $r = 0.06$ salt-in-PEO mixture for electrostatic force exerted on of all partial charges in the system ('field', i.e. including the polymer atoms' partial charges) and ionic charge carriers only ('acceleration', i.e. lithium and TFSI only).

S6: Structure formation principle - s_{asym} analysis

As mentioned in the main body of the paper we provide additional information on the chain ordering and coordination pattern for lithium on the polymer backbone. The observables used for this matter are the number of lithium ions coordinated to the backbone n_{backbone} , the asymmetry of their coordination sites as captured by s_{asym} , the polymer chain's mean-squared gyration radius $R_{g,z}^2$ in field direction and the number of monomers coordinating lithium.

We propose an explanatory model for the coiled-to-stretched transformation of the polymer conformation upon increasing field strength with the underlying idea of lithium, closely attached to the ether oxygens, pulling the polymer chain into the elongated shape. Therefore, we define an order parameter s_{asym} that quantifies the degree of symmetry of the lithium coordination of a chain:

$$s_{\text{asym}} = \frac{|n_{\text{Li}} - (N - 1)/2|}{(N - 1)/2}, \quad (1)$$

where n_{Li} denotes the average index of the monomers coordinating the lithium ions on the individual chain and N is the total number of monomers of a chain. For example, for a symmetric coordination of a single lithium ion to the chain center the definition yields $s_{\text{asym}} = 0$, whereas coordination to the outermost monomer at the chain end $s_{\text{asym}} = 1$. We assume that the stretching is most effective when lithium exerts such a pulling force at the chain ends. To be most sensitive to this effect, we determine $R_{g,z}^2$ as a function of s_{asym} for a subensemble where only a single lithium ion is attached to the polymer chain. The correlations between s_{asym} and $R_{g,z}^2$ are shown in Figure S14.

We make two independent observations:

First, we note that $R_{g,z}^2$ increases for increasing s_{asym} in absence of an external field. For coordination of lithium at a center position the chain loops in the crown-ether fashion which thus results in a more coiled conformation. For a lithium - chain end contact, the ether oxygen coordination number drops (see Figure S17) and the coiling effect due to lithium becomes smaller. Second, we observe a dramatic stretching effect for increasing E_z for increasing

s_{asym} , which resonates well with our assumption of lithium-induced stretching. The fact that also $R_{g,z}^2$ for $s_{\text{asym}} = 0$ shifts to higher values, we attribute to a local stretching as visually illustrated in the simulation snapshots in Figure S14 as well as the ordering effect of adjacent stretched chains.

On that basis, the previous observation of more effective chain alignment in field direction for decreasing salt content can be understood as a mere concentration effect. As can be seen in Figure S20 the probability for an asymmetric distribution of the lithium ions on the polymer backbone decreases with increasing salt content and so does consequently the ability of the lithium ions to stretch the chains.

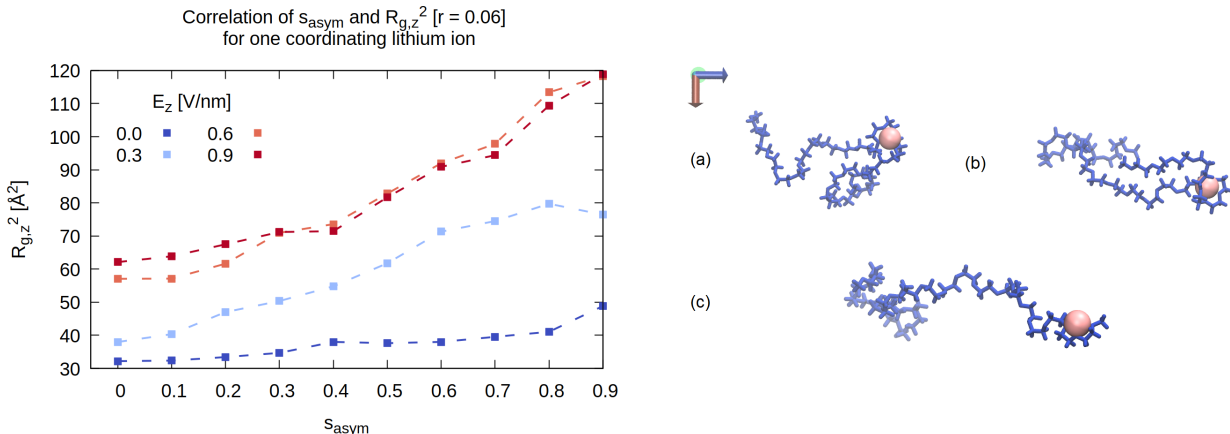


Figure S14: Left: Relation between squared gyration radius in field direction $R_{g,z}^2$ and asymmetric chain coordination parameter s_{asym} for various electric field strengths exemplary for the $r = 0.06$ mixture. Right: Illustration of lithium induced stretching of the polymer chain. The snapshots are taken from the $E_z = 1.0$ V/nm simulation of the $r = 0.06$ mixture. For (a) $s_{\text{asym}} = 0.0$ and $R_{g,z}^2 = 58 \text{ \AA}^2$, (b) $s_{\text{asym}} = 0.5$ and $R_{g,z}^2 = 85 \text{ \AA}^2$ and (c) $s_{\text{asym}} = 0.9$ and $R_{g,z}^2 = 130 \text{ \AA}^2$.

Figure S15 shows the correlation of $R_{g,z}^2$ and s_{asym} in consideration of all possible lithium coordination motifs to the polymer backbone, i.e. all possible n_{backbone} , and not only the subensemble of $n_{\text{backbone}} = 1$ as discussed previously. Our underlying intention was to fairly compare the lithium-chain-dragging mechanism across the field range via this correlation while we remain aware of the significant change of the local polymer environment of lithium.

Having said this, the relation between $R_{g,z}^2$ and s_{asym} are recovered qualitatively for the complete ensemble of n_{backbone} .

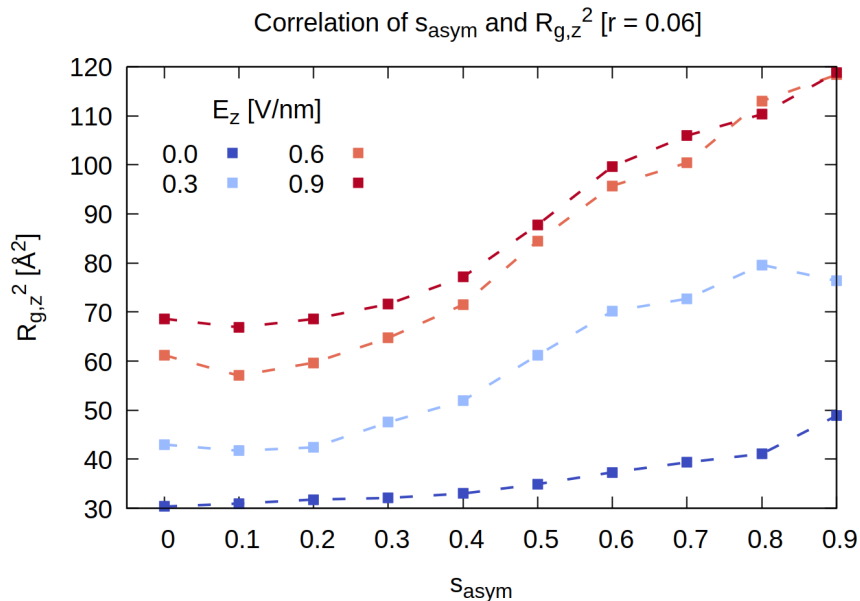


Figure S15: Effect of E_z on $R_{g,z}^2$ binned according to the asymmetry s_{asym} of lithium coordination to backbone for taking into account all possible lithium coordination motifs, i.e. not only the subset of a single lithium coordinating to the backbone.

In Figure S16 we show the correlation between $R_{g,z}^2$ and n_{backbone} for various field strengths. We observe a shift of $R_{g,z}^2$ to higher values even when there is no lithium coordinating to the chain, i.e. $n_{\text{backbone}} = 0$. As mentioned in before, we interpret this as indicative of the ordering effect of stretched chains. Note that in absence of an external field, the equilibrium $R_{g,z}^2$ of the plain polymer melt is recovered for $n_{\text{backbone}} = 0$.

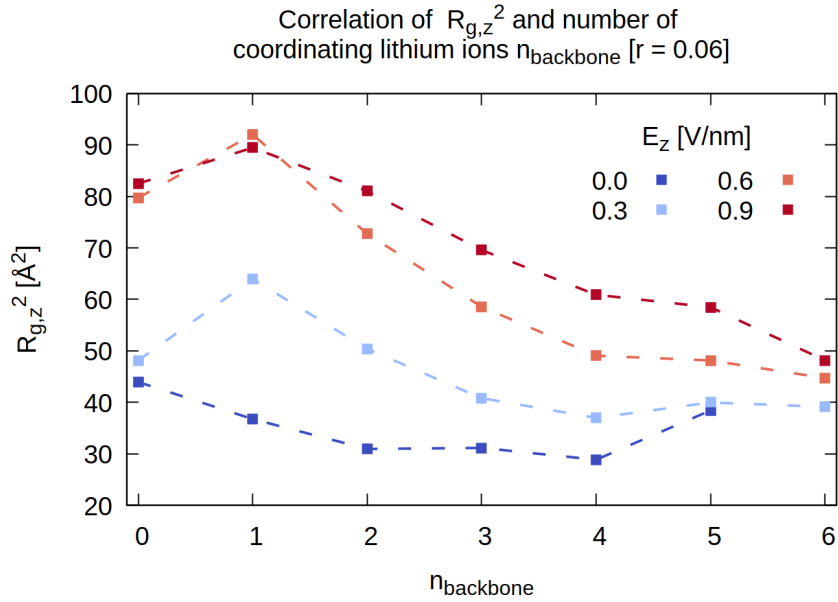


Figure S16: Average $R_{g,z}^2$ as a function of the number of lithium coordinated to the polymer chain for various field strengths.

In Figure S17 we show how the average number of ether oxygens CN, provided by one chain, coordinating lithium changes as a function of s_{asym} and electric field. Firstly, we observe that CN shifts to lower values for increasing field strength which can be explained by the progressing detachment of lithium from the polymer backbone. Secondly, we note a slight increase of CN for $s_{\text{asym}} = 0.8$ followed by a steep drop to $\text{CN} = 1$ for $s_{\text{asym}} = 1$. Whereas for $s_{\text{asym}} = 0.8$ the loose end of the polymer chain can wrap lithium efficiently, a maximum asymmetric position of lithium on the polymer backbone naturally corresponds to a single monomer contact.

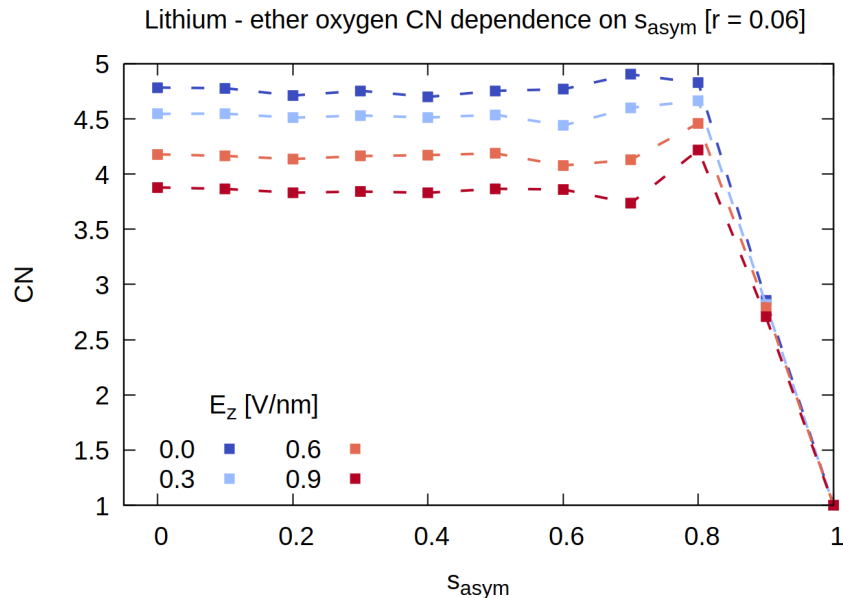


Figure S17: Average lithium coordination via ether oxygens as a function of asymmetry of lithium coordination to the backbone for various field strengths.

Figure S18 provides information on the composition of the individual s_{asym} values. While a very asymmetric lithium coordination of the backbone is usually provided by a single lithium ion attached at an outer position, a symmetric coordination of the chain is on average constituted via 2 or 3 lithium ions positioned on the chain. We further note an upshift of the number of lithium ions coordinated to the polymer chain n_{backbone} for increasing field strength. We attribute this effect to the more frequent coordination of lithium via 2 chains as discussed in the main text. Consequently, polymer chains may increasingly share the same lithium ion.

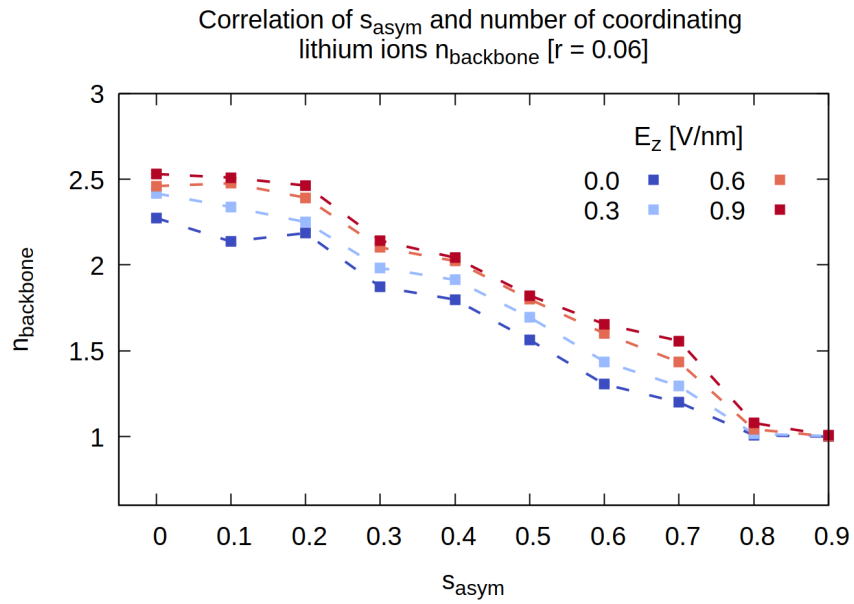


Figure S18: Effect of E_z on the average number of lithium ions on the backbone constituting the respective s_{asym} .

Figure S19 shows the probability distribution of s_{asym} . The favorable wrapping of the polymer chain tail around lithium at $s_{\text{asym}} = 0.8$ emerges as more frequent. The lithium-chain-dragging in field direction is further reflected in a slight increase of asymmetric coordination for increasing E_z .

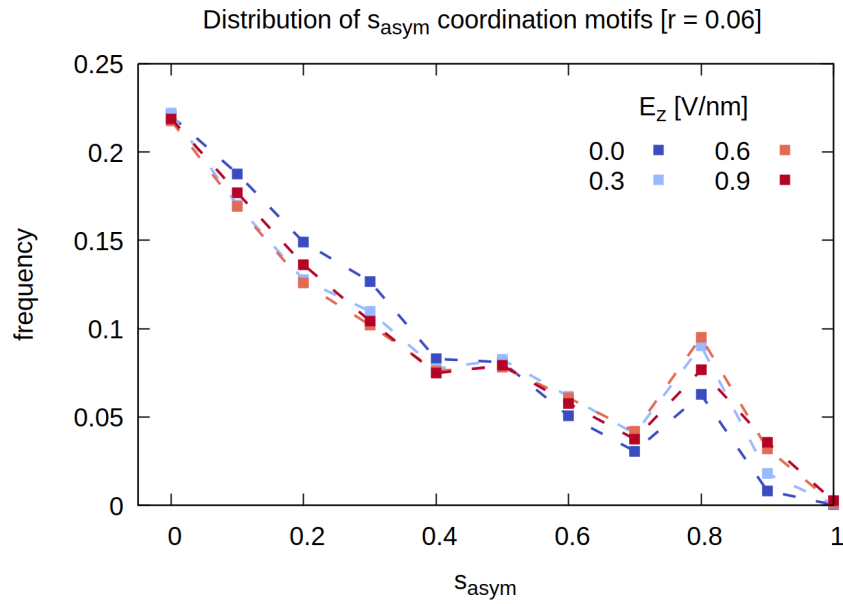


Figure S19: Effect of E_z on the probability distribution of s_{asym} . An entirely asymmetric coordination, i.e. $s_{\text{asym}} = 1.0$ is observed in less than 0.25% of the samples.

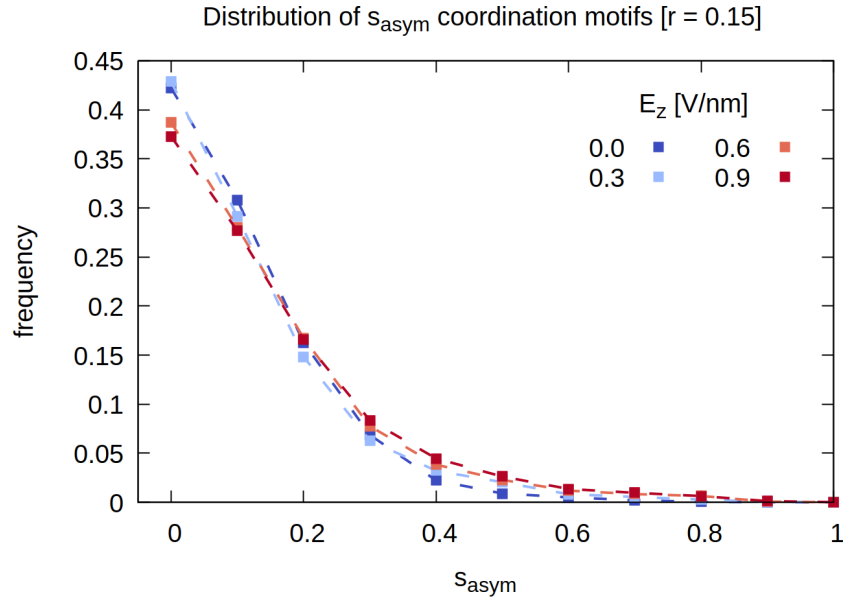


Figure S20: Effect of E_z on the probability distribution of s_{asym} for the salt content $r = 0.15$.

S7: Structural and dynamic response for chain length $N = 54$

Simulation of polymeric electrolytes by means of all-atomistic molecular dynamics is a challenging task due to the slow dynamics of the lithium ions, which strongly interact with the ether oxygens of the polymer backbone, and the long relaxation times of the polymer. Hence, atomistic-level simulation of such systems comes along at extensive computational cost. To assess within the frame of computational capabilities if the response of the polymer electrolyte system is qualitatively affected by the chain length, we performed additional simulations of the $r = 0.06$ mixture but employing chains of double the length $N = 54$. We extended the equilibration run to 500 ns followed by simulation for data acquisition with a duration of $2 \mu\text{s}$ for $E_z < 0.6 \text{ V/nm}$ and $1 \mu\text{s}$ for the remaining field strengths.

In Figure S21 we show the response of $R_{g,z}^2$ for both chain lengths. For the chain length $N = 54$ $R_{g,z}^2$ plateaus at $E_z > 0.4 \text{ V/nm}$. We note that the correlation between stretching of the polymer chains in direction of the electric field and asymmetric lithium coordination holds also for $N = 54$ (see Figure S22). We assume that the coiled-to-stretched transformation is more pronounced for $N = 54$, because the stretching is more efficient for lithium exerting a pulling force on the chain end.

In Figures S23 and S24 it is shown that the nonlinear effects for μ and D_{\parallel} occur for longer chains as well. As known from experimental and theoretical literature^{36–38} transport properties decrease in magnitude for increasing chain length.

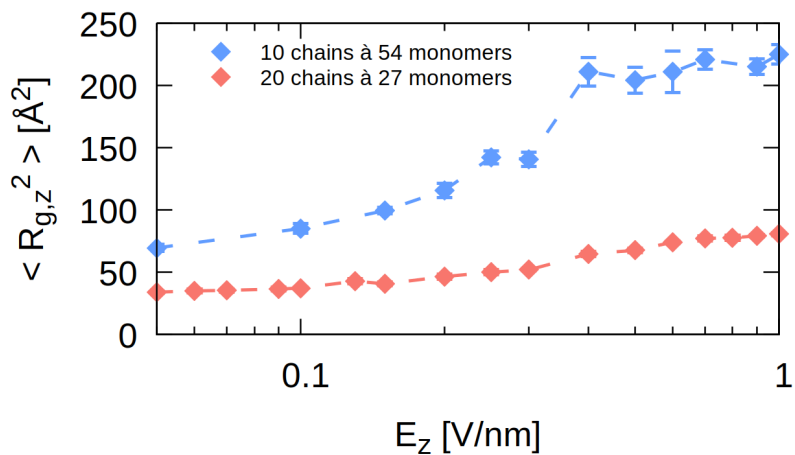


Figure S21: Comparison of $R_{g,z}^2$ as a function of electric field strength for two different polymer chain lengths.

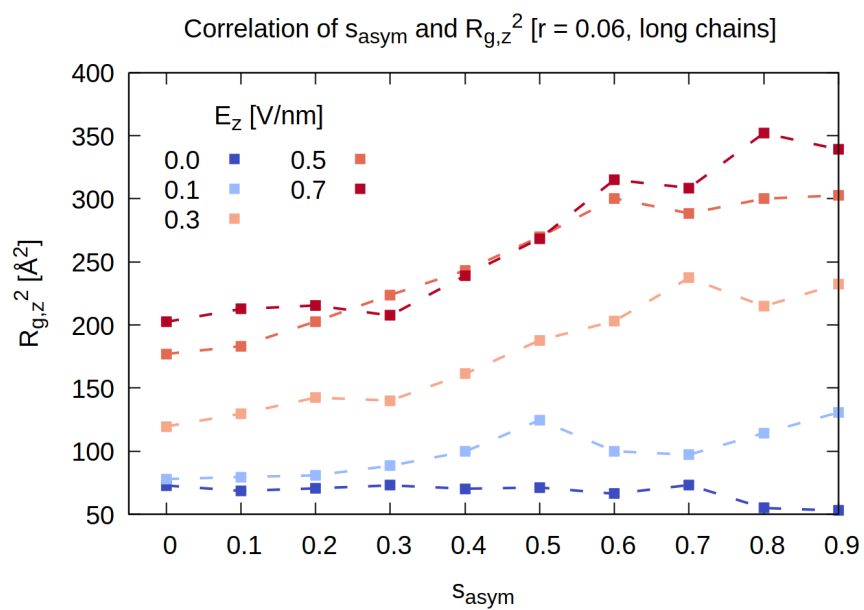


Figure S22: Effect of E_z on $R_{g,z}^2$ binned according to the asymmetry s_{asym} of lithium coordination to backbone for the $r=0.06$ system containing chains of the length $N=54$.

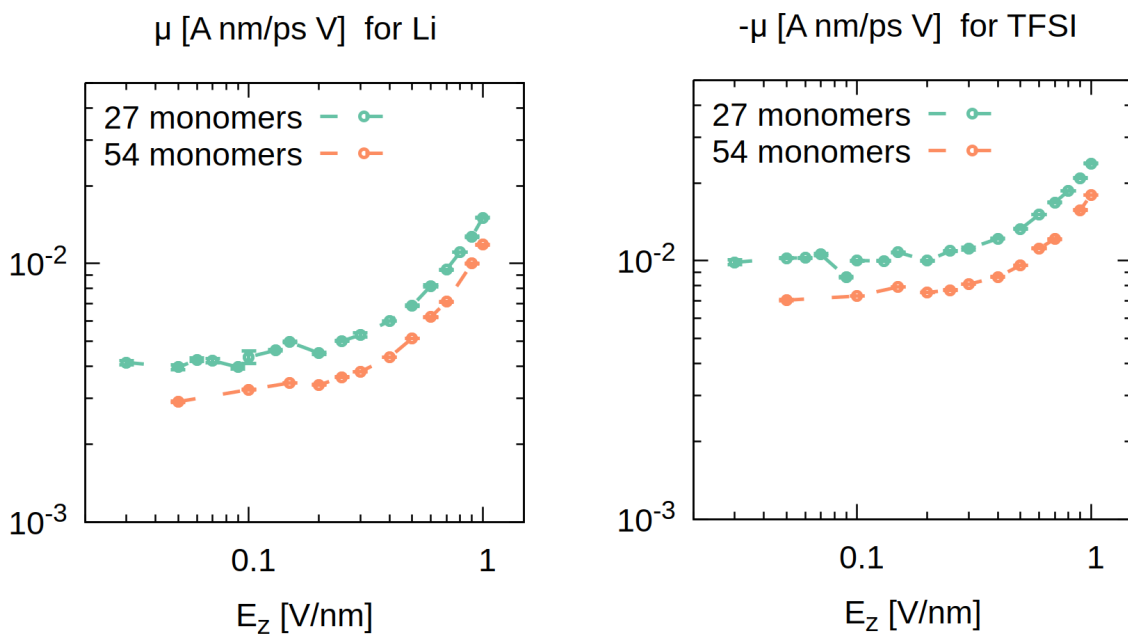


Figure S23: Comparison of lithium and TFSI mobilities μ as a function of electric field strength for two different polymer chain lengths.

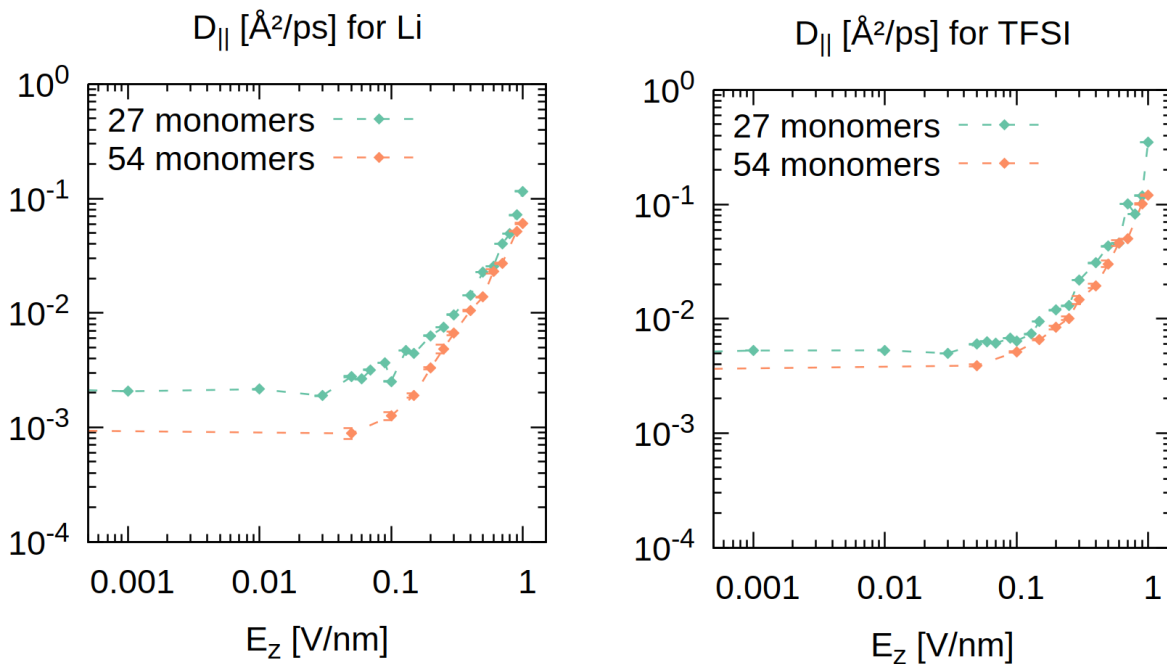


Figure S24: Comparison of lithium and TFSI diffusion coefficients $D_{||}$ as a function of electric field strength for two different polymer chain lengths.

S8: Switching field from $E_z = 0.0$ to 1.0 V/nm

We investigated the process of equilibration of structural and dynamic observables in response to field application for the $r = 0.06$ electrolyte system. To track the temporal evolution with sufficient statistics, we conducted a simulation series consisting of 100 short individual runs. The simulation protocol for the individual runs splits up in three steps:

(1) The starting configurations were extracted from the $E_z = 0.0$ V/nm trajectory 18 ns apart from each other.

(2) A sudden tilting of the potential energy surface may cause ions to immediately slip into their accordingly shifted local energy minima, thus provoking high instantaneous velocities of the particles. To separate this only initially effective increase of ionic motion from an enhancement of steady-state transport properties due to tilting or a structurally conditioned enhancement (see introductory sketch Figure 1 as well as sketch Figure 8), we generated a set of simulations preceded by three different equilibration protocols. Firstly, we performed production runs for direct application of $E_z = 1.0$ V/nm on the unperturbed $E_z = 0.0$ V/nm structures ('no restraints prior to production run' in Figure S25). Secondly, to permit the ions' adjustment to the newly shifted local energy minima due to $E_z = 1.0$ V/nm in an otherwise unchanged structural environment, we interposed a restrained equilibration run. The positions of the polymer backbone atoms were restrained in all directions by means of a harmonic potential with a force constant of 400.00 kJ/mol. This restrained equilibration was carried out for either 20 ps or 1 ns at an integration time step of 0.5 fs ('restrained polymer chains for 1 ns / 20 ps prior to production run' in Figure S25).

(3) The production run for data acquisition was carried out for 5 ns (respectively 1 ns for the unrestrained / 20 ps long restrained equilibration setup) using the same simulation parameters as for the previous steady-state simulations. The data was then averaged over all individual simulations.

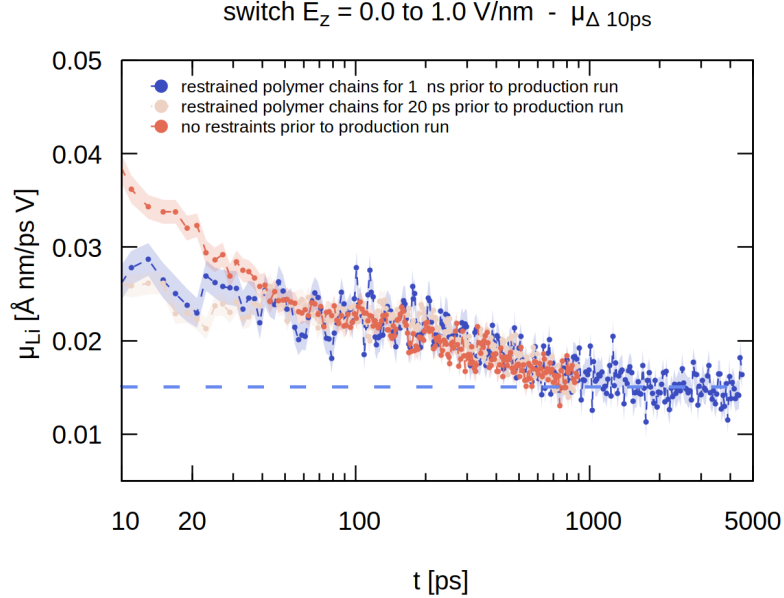


Figure S25: Lithium mobility as a function of simulation time for different equilibration procedures prior to the production run. The dashed line represents the stationary state μ_{Li} for $E_z = 1.0 \text{ V/nm}$.

In Figure S25, we show the impact of freezing the chain structure prior to the production run on $\mu_{\text{Li}}(t)$. As discussed before the sudden tilting of the energy landscape causes the ions to quickly slip into their new local energy minima and thus translates into an elevated velocity in field direction (see 'no restraints') for short times after the field has been switched on. We observe that the increase of the initial $\mu_{\text{Li}}(t)$ is smaller for prior restraints on the polymer chains and an equilibration duration of both 20 ps and 1 ns quantitatively yields the same behavior. We rationalize this by a fast local adjustment of the ions to the local energy minima during the restrained pre-equilibration.

As introduced in the main text, we measure the instantaneous mobility $\mu(t)$ as:

$$\mu(t) = \frac{\langle \nu(t) \rangle}{E} = \frac{1}{E \cdot \Delta t} \left(\left\langle z \left(t + \frac{\Delta t}{2} \right) \right\rangle - \left\langle z \left(t - \frac{\Delta t}{2} \right) \right\rangle \right), \quad (2)$$

the drift velocity is thus evaluated for a constant time lag Δt between the reference positions. For short time lags Δt it is crucial to gather data with sufficient statistics because the

drift motion is overlaid by thermal noise. We compare extracting $\mu(t)$ via equation (2) for $\Delta t = 10$ ps to extracting the current velocity ν from the numerical derivative of the lithium displacement in field direction $\Delta z_{\text{Li}}(t)$ in Figure S26. We show that the noise can be reduced for increasing Δt .

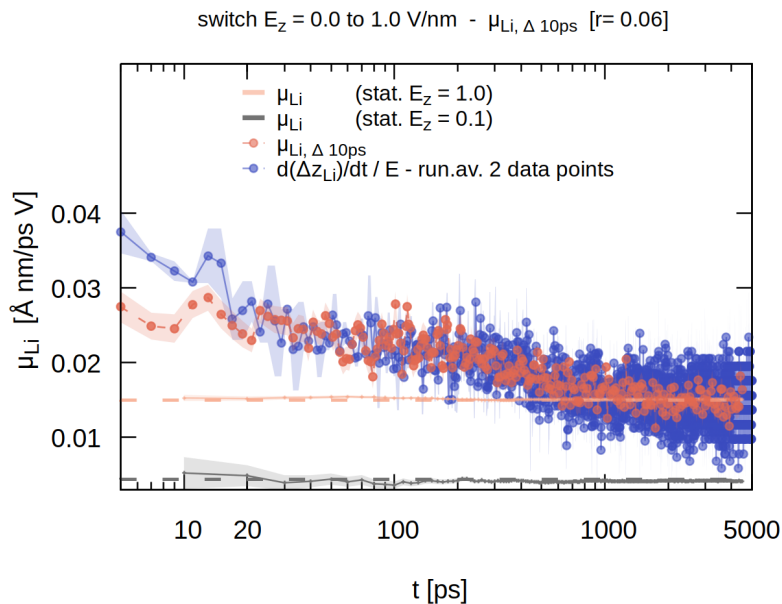


Figure S26: Lithium mobility as a function of simulation time since the polymer chains are released from positional restraints for either obtaining μ_{Li} from the numerical derivative of $d(\Delta z_{\text{Li}})/dt$ or at a constant time lag of $\Delta 10$ ps. The dashed lines represent the stationary state μ_{Li} for $E_z = 0.1$ V/nm in the linear response regime, respectively $E_z = 1.0$ V/nm. The lag time dependence of μ_{Li} in the stationary state simulations is shown in the corresponding colors as well (μ_{stat} not shown as a function of simulation time but lag time to compute μ_{stat}).

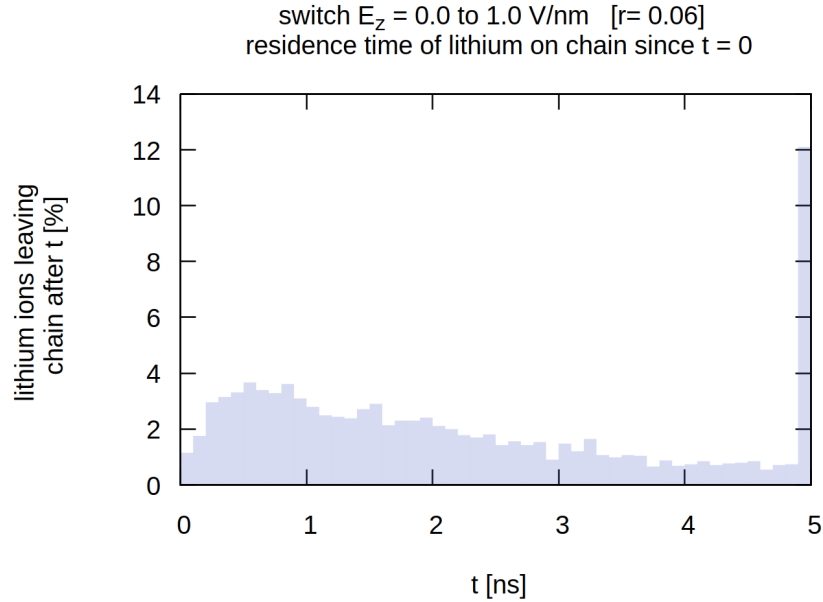


Figure S27: Distribution of residence times of lithium on the polymer chains that lithium is attached to at $t=0$ ps. Since the simulations are 5 ns long, the last data bar must be understood to mean that after 5 ns 12% of initial lithium-chain-pairs are still preserved.

The long time limit of the overall $\Delta\tilde{z}_{\text{Li-PEO}}$ effectively is a complex interplay of different effects: lithium transfers between chains and further the system comprises diverse coordination scenarios, for example lithium binding to multiple polymer chains or a polymer chain hosting multiple lithium ions (see Figure 28 for taking all lithium-chain-pairs into consideration).

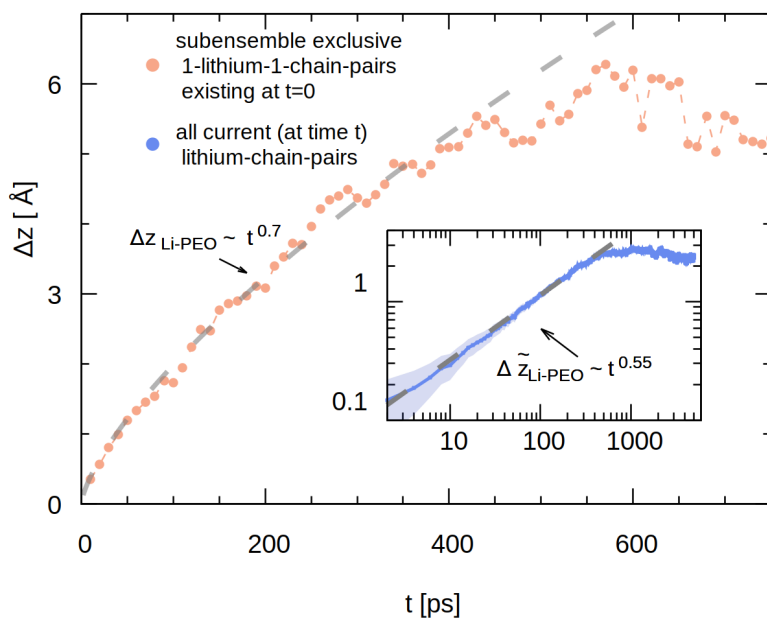


Figure S28: As displayed in the main Figure 14: Time evolution of lithium displacement relative to the center of mass of the polymer chain, that it is attached to, $\Delta z_{\text{Li-PEO}}$ for the subensemble of distinct lithium-chain-pairs existent at $t = 0$ ps, where lithium coordinates to a single chain and the chain is coordinated exclusively by this lithium ion. The inset shows the same analysis for $\Delta \tilde{z}_{\text{Li-PEO}}$ including all lithium-chain pairs that are present at time t .

References

- (1) Berendsen, H. J.; van der Spoel, D.; van Drunen, R. GROMACS: A message-passing parallel molecular dynamics implementation. *Computer Physics Communications* **1995**, *91*, 43–56.
- (2) Van Der Spoel, D.; Lindahl, E.; Hess, B.; Groenhof, G.; Mark, A. E.; Berendsen, H. J. GROMACS: Fast, flexible, and free. *Journal of Computational Chemistry* **2005**, *26*, 1701–1718.
- (3) Páll, S.; Abraham, M. J.; Kutzner, C.; Hess, B.; Lindahl, E. Tackling exascale software challenges in molecular dynamics simulations with GROMACS. Lecture Notes in Computer Science (including subseries Lecture Notes in Artificial Intelligence and Lecture Notes in Bioinformatics). 2015; pp 3–27.
- (4) Abraham, M. J.; Murtola, T.; Schulz, R.; Páll, S.; Smith, J. C.; Hess, B.; Lindahl, E. Gromacs: High performance molecular simulations through multi-level parallelism from laptops to supercomputers. *SoftwareX* **2015**, *1-2*, 19–25.
- (5) Jorgensen, W. L.; Maxwell, D. S.; Tirado-Rives, J. Development and testing of the OPLS all-atom force field on conformational energetics and properties of organic liquids. *Journal of the American Chemical Society* **1996**, *118*, 11225–11236.
- (6) Canongia Lopes, J. N.; Padua, A. A. CL&P: A generic and systematic force field for ionic liquids modeling. *Theoretical Chemistry Accounts* **2012**, *131*, 1–11.
- (7) Canongia Lopes, J. N.; Deschamps, J.; Padua, A. A. H. Modeling Ionic Liquids Using a Systematic All-Atom Force Field. *The Journal of Physical Chemistry B* **2004**, *108*, 2038–2047.
- (8) Lopes, J. N.; Padua, A. A. Molecular force field for ionic liquids composed of triflate or bistriflylimide anions. *Journal of Physical Chemistry B* **2004**, *108*, 16893–16898.

- (9) Shimizu, K.; Almantariotis, D.; Costa Gomes, M. F.; Pádua, A. A.; Canon-gia Lopes, J. N. Molecular force field for ionic liquids V: Hydroxyethylimi-dazolium, dimethoxy-2methylimidazolium, and fluoroalkylimidazolium cations and Bis(fluorosulfonyl)amide, perfluoroalkanesulfonylamide, and fluoroalkylfluorophos-phate anions. *Journal of Physical Chemistry B* **2010**, *114*, 3592–3600.
- (10) Salanne, M. Simulations of room temperature ionic liquids: From polarizable to coarse-grained force fields. *Physical Chemistry Chemical Physics* **2015**, *17*, 14270–14279.
- (11) Nasrabadi, A. T.; Gelb, L. D. Structural and Transport Properties of Tertiary Ammo-nium Triflate Ionic Liquids: A Molecular Dynamics Study. *Journal of Physical Chem-istry B* **2017**, *121*, 1908–1921.
- (12) Dommert, F.; Wendler, K.; Berger, R.; Delle Site, L.; Holm, C. Force fields for studying the structure and dynamics of ionic liquids: A critical review of recent developments. *ChemPhysChem* **2012**, *13*, 1625–1637.
- (13) Leontyev, I. V.; Stuchebrukhov, A. A. Polarizable molecular interactions in condensed phase and their equivalent nonpolarizable models. *Journal of Chemical Physics* **2014**, *141*, 014103.
- (14) Leontyev, I.; Stuchebrukhov, A. Accounting for electronic polarization in non-polarizable force fields. *Physical Chemistry Chemical Physics* **2011**, *13*, 2613–2626.
- (15) Youngs, T. G.; Hardacre, C. Application of static charge transfer within an ionic-liquid force field and its effect on structure and dynamics. *ChemPhysChem* **2008**, *9*, 1548–1558.
- (16) Müller-Plathe, F.; van Gunsteren, W. F. Computer simulation of a polymer electrolyte: Lithium iodide in amorphous poly(ethylene oxide). *The Journal of Chemical Physics* **1995**, *103*, 4745–4756.

- (17) Costa, L. T.; Sun, B.; Jeschull, F.; Brandell, D. Polymer-ionic liquid ternary systems for Li-battery electrolytes: Molecular dynamics studies of LiTFSI in a EMIm-TFSI and PEO blend. *Journal of Chemical Physics* **2015**, *143*, 024904.
- (18) Mogurampelly, S.; Keith, J. R.; Ganesan, V. Mechanisms Underlying Ion Transport in Polymerized Ionic Liquids. *Journal of the American Chemical Society* **2017**, *139*, 9511–9514.
- (19) Mogurampelly, S.; Ganesan, V. Structure and mechanisms underlying ion transport in ternary polymer electrolytes containing ionic liquids. *The Journal of Chemical Physics* **2017**, *146*, 074902.
- (20) Sunda, A. P.; Mondal, A.; Balasubramanian, S. Atomistic simulations of ammonium-based protic ionic liquids: steric effects on structure, low frequency vibrational modes and electrical conductivity. *Physical Chemistry Chemical Physics* **2015**, *17*, 4625–4633.
- (21) Mondal, A.; Balasubramanian, S. Quantitative Prediction of Physical Properties of Imidazolium Based Room Temperature Ionic Liquids through Determination of Condensed Phase Site Charges: A Refined Force Field. *The Journal of Physical Chemistry B* **2014**, *118*, 3409–3422.
- (22) Bhargava, B. L.; Balasubramanian, S. Refined potential model for atomistic simulations of ionic liquid [bmim][PF₆]. *The Journal of Chemical Physics* **2007**, *127*, 114510.
- (23) Chaban, V. V.; Voroshylova, I. V.; Kalugin, O. N. A new force field model for the simulation of transport properties of imidazolium-based ionic liquids. *Physical Chemistry Chemical Physics* **2011**, *13*, 7910.
- (24) Borodin, O.; Smith, G. D. Molecular Dynamics Simulations of Poly(ethylene oxide)/LiI Melts. 2. Dynamic Properties. **2000**,

- (25) Borodin, O.; Smith, G. D. Mechanism of Ion Transport in Amorphous Poly(ethylene oxide)/LiTFSI from Molecular Dynamics Simulations. *Macromolecules* **2006**, *39*, 1620–1629.
- (26) Martinez, L.; Andrade, R.; Birgin, E. G.; Martínez, J. M. PACKMOL: A package for building initial configurations for molecular dynamics simulations. *Journal of Computational Chemistry* **2009**, *30*, 2157–2164.
- (27) Berendsen, H. J. C.; Postma, J. P. M.; van Gunsteren, W. F.; DiNola, A.; Haak, J. R. Molecular dynamics with coupling to an external bath. *The Journal of Chemical Physics* **1984**, *81*, 3684–3690.
- (28) Bussi, G.; Donadio, D.; Parrinello, M. Canonical sampling through velocity rescaling. *The Journal of Chemical Physics* **2007**, *126*, 014101.
- (29) Hess, B.; Bekker, H.; Berendsen, H. J. C.; Fraaije, J. G. E. M. LINCS: A linear constraint solver for molecular simulations. *Journal of Computational Chemistry* **1997**, *18*, 1463–1472.
- (30) Hess, B. P LINCS:A Parallel Linear Constraint Solver for Molecular Simulation. **2007**,
- (31) Parrinello, M.; Rahman, A. Polymorphic transitions in single crystals: A new molecular dynamics method. *Journal of Applied Physics* **1981**, *52*, 7182–7190.
- (32) Nosé, S.; Klein, M. Constant pressure molecular dynamics for molecular systems. *Molecular Physics* **1983**, *50*, 1055–1076.
- (33) Nosé, S. A molecular dynamics method for simulations in the canonical ensemble. *Molecular Physics* **1984**, *52*, 255–268.
- (34) Hoover, W. G. Canonical dynamics: Equilibrium phase-space distributions. *Physical Review A* **1985**, *31*, 1695–1697.

- (35) Xu, K. Nonaqueous Liquid Electrolytes for Lithium-Based Rechargeable Batteries. *Chemical reviews* **2004**, *104*, 4303–4418.
- (36) Timachova, K.; Watanabe, H.; Balsara, N. Effect of Molecular Weight and Salt Concentration on Ion Transport and the Transference Number in Polymer Electrolytes. *Macromolecules* **2015**, *48*, 7882–7888.
- (37) Brooks, D. J.; Merinov, B.; Goddard, W.; Kozinsky, B.; Mailoa, J. Atomistic Description of Ionic Diffusion in PEOLiTFSI: Effect of Temperature, Molecular Weight, and Ionic Concentration. *Macromolecules* **2018**, *51*, 8987–8995.
- (38) Chatteraj, J.; Knappe, M.; Heuer, A. Dependence of Ion Dynamics on the Polymer Chain Length in Poly(ethylene oxide)-Based Polymer Electrolytes. *The Journal of Physical Chemistry B* **2015**, *119*, 6786–6791.